Energy-Flow Tomography of QCD: Correlators across Confinement, Matter, and Spin

Xiaohui Liu[a,b], Ian Moult[c] and Hua Xing Zhu[d,e,b]
[a]School of Physics and Astronomy, Beijing Normal University, and Key Laboratory of Multiscale Spin Physics (Beijing Normal University), Ministry of Education, Beijing 100875, China,
[b]Southern Center for Nuclear Science Theory (SCNT), Institute of Modern Physics, Chinese Academy of Science, Huizhou 516000, China,
[c]Department of Physics, Yale University, New Haven, CT 06511, USA,
[d]School of Physics, Peking University, Beijing 100871, China,
[e]Center for High Energy Physics, Peking University, Beijing 100871, China.

Contents

Abstract

Patterns of energy flow in high-energy final states are shaped by hadronization and confinement dynamics, nuclear-matter effects, and the spin and flavor structure of hadrons. Measuring these patterns exposes how nonperturbative QCD reorganizes short-distance radiation into correlated hadronic energy flow. Energy correlators provide an infrared-safe and correlation-based way to read this information. Their light-ray operator structure connects collider observables to modern OPE methods and opens new windows on nonperturbative QCD dynamics. Jet substructure provides a more traditional route to the same energy-flow information inside jets. Together, these observables turn final-state radiation patterns into probes of hadronization, confinement, nuclear matter, hadron structure, and spin dynamics.

Keywords: Energy correlators; energy flow; jet substructure; confinement; hadronization; nuclear matter; hadron structure; spin physics; light-ray OPE; power-correction; di-hadron fragmentation; transverse-momentum-dependent factorization.

1 Introduction

The distribution of energy in a high-energy final state is one of the most direct experimental records of QCD radiation. Although it is measured after hadronization, its angular structure retains information about the dynamics that produced and reshaped the radiation, from perturbative branching to confinement, nuclear interactions, and spin-dependent correlations. This review describes recent progress in using energy-flow measurements as quantitative probes of these aspects of QCD.

Two related developments have made this connection especially useful. Jet substructure [1, 2] provides controlled ways to select and identify radiation inside jets, while energy correlators [3] measure energy-weighted angular correlations in the same final states with a direct operator interpretation. This combination connects experimentally resolved jet measurements with QCD dynamics ranging from perturbative evolution to hadronization, nuclear effects, and spin-dependent correlations.

2 Energy Correlators and Novel Jet Substructure Methods

2.1 Energy Correlators

Energy correlators were introduced in QCD by Basham, Brown, Ellis, and Love in the study of e^+e^- annihilation, where weighted angular correlations of final-state energy flow were proposed as infrared-safe probes of asymptotic freedom [4, 5]. In recent years, energy correlators have undergone a renewed development driven by converging progress in quantum field theory, perturbative QCD, nuclear physics, and

collider measurements [3]. The conformal-collider analysis of Hofman and Maldacena placed energy-flow correlations in a light-ray-operator framework and showed that their small-angle singularities are controlled by nonlocal light-ray operators of definite spin [6, 7]. In perturbative QCD, the small-angle limit is controlled by collinear evolution and admits an anomalous-dimension governed scaling law [8, 9]. Recent theoretical and experimental work has shown that this near-side region contains more than the asymptotic perturbative region. As the angular scale is lowered, the correlator passes through a parton-hadron transition region and into a post-confinement regime governed by genuinely nonperturbative di-hadron fragmentation dynamics [3, 10–20]. The opposite endpoint, the back-to-back limit, is governed by transverse recoil and factorizes in the same transverse-momentum space that appears in standard TMD factorization [21–23]. The near-side and back-to-back endpoints therefore probe different infrared limits of the same energy-flow correlator, collinear evolution and hadronization for the small angle limit, and recoil-sensitive TMD dynamics for almost back-to-back configuration. Measurements at LEP, RHIC, and the LHC have used these two limits to extract α_s, identify angular transition scales, test hadronization models, and quantify medium-induced modifications in nuclear collisions [11, 12, 24–28]. The same energy-flow construction has also been adapted to hadron structure, spin physics, and small-x dynamics. Examples include nucleon energy correlators (NECs) [29–34], semi-inclusive energy correlators (SIECs) [35–37], one-point energy correlators (OPECs) [38–45], and transverse energy-energy correlators (TEECs) [46–52].

2.1.1 Standard EEC: definitions, kinematics, and regime structure

The standard EEC is defined as the correlation function of two energy-flow operators inserted between states created by a hard source [6],

$$\mathrm{EEC} = \frac{\int d^4x\, e^{iq\cdot x}\,\langle 0|O^\dagger(x)\,\mathcal{E}(\hat{n}_1)\,\mathcal{E}(\hat{n}_2)\,O(0)|0\rangle}{Q^2\int d^4x\, e^{iq\cdot x}\,\langle 0|O^\dagger(x)\,O(0)|0\rangle}\,, \tag{1}$$

where O denotes the hard source, such as the electromagnetic current J^μ. Here, q^μ is the total timelike momentum injected into the system, and $Q \equiv \sqrt{q^2}$. The operators $\mathcal{E}(\hat{n}_1)$ and $\mathcal{E}(\hat{n}_2)$ measure the energy flux through detectors oriented along $\hat{n}_1$ and $\hat{n}_2$. The detector operator is [53]

$$\mathcal{E}(\hat{n}) = \int_0^\infty dt\, \lim_{r\to\infty} r^2 n^i T^{0i}(t, r\hat{n}), \tag{2}$$

which is the standard light-ray transform of the energy-momentum tensor in the direction $\hat{n}$ [6]. This operator definition could be implemented directly on future quantum computers; for pioneering studies, see Ref. [54–56]. Higher-point energy correlators (ENC) are obtained by inserting additional energy-flow operators and have found broad applications in collider physics [10, 57–64]. Energy correlators can also be made quantum-number resolved by restricting the energy flow to hadrons carrying specified charges, flavors, or other labels, providing more differential probes of hadronization and heavy-flavor dynamics [57, 65–69].

Using a completeness relation, Eq. (1) can be rewritten in the familiar event-level form [1]

$$\frac{d\Sigma}{d\chi} = \sum_{i,j}\int \frac{d\sigma_{ij}}{\sigma}\,\frac{E_iE_j}{Q^2}\,\delta(\chi-\theta_{ij})\,, \tag{3}$$

where σ is the inclusive cross section. The sum runs over final-state hadrons i and j, E_i and E_j are their energies, and θ_{ij} is their opening angle. In hadronic collisions, the EEC can be generalized to the transverse-energy-weighted cross section differential in the azimuthal separation, leading to the TEEC observable [46]. The final-state hadrons may be selected inclusively, within jets, or on tracks [57, 66], with the last option offering superior angular resolution. For later discussion, it is convenient to introduce

$$z = \frac{1-\cos\chi}{2}\,. \tag{4}$$

Figure 1 shows the LEP measurement of the EEC in e^+e^- annihilation using tracks over the full angular range, which provides a direct scan of the physics probed at different angular separations. In the central part of the distribution, the relevant scale remains of order Q, and the EEC is described quantitatively by perturbation theory [71–73] up to hadronization power corrections.

Toward the small-angle side, the relevant transverse scale decreases as $Q\chi/2 \sim Q\sqrt{z}$, and the correlator resolves collinear dynamics. On this side, the EEC exhibits a nontrivial scaling law, first discovered by Hofman and Maldacena [6], who argued in conformal field theory that the small-angle singularity of energy correlators is controlled by light-ray operators of definite spin, and the near-side distribution takes a pure power law, giving the original conformal-collider picture of angular scaling [6]. Later in QCD, this structure is realized in a more quantitative form. The small-z limit admits a leading-power factorization theorem together with all-order resummation, so that the asymptotic EEC can be written as a perturbative scaling law whose exponent is determined by the relevant moments of the timelike splitting functions [8]. The singular behavior as $z \to 0$ is therefore predicted order by order by collinear QCD evolution.

The LEP data in Fig. 1, however, shows that this perturbative scaling law cannot persist down to arbitrarily small z. The near-side spectrum contains more than one domain. At moderately small z, the distribution follows the perturbative scaling regime. Further toward $z \to 0$, the data enter a transition region before reaching a post-confinement domain with a different scaling pattern. The departure from the perturbative small-z law marks the onset of nonperturbative dynamics.

[1] The original EEC introduced in Refs. [4, 5] was fully differential in the relevant angles, with additional dependence on θ and ϕ, where θ denotes the opening angle between one energy flow (i) and the beam, and ϕ denotes the azimuthal angle of energy flow j relative to the plane spanned by the beam and energy flow i. This additional angular information is later found to be relevant for hadron spin structure studies [70].

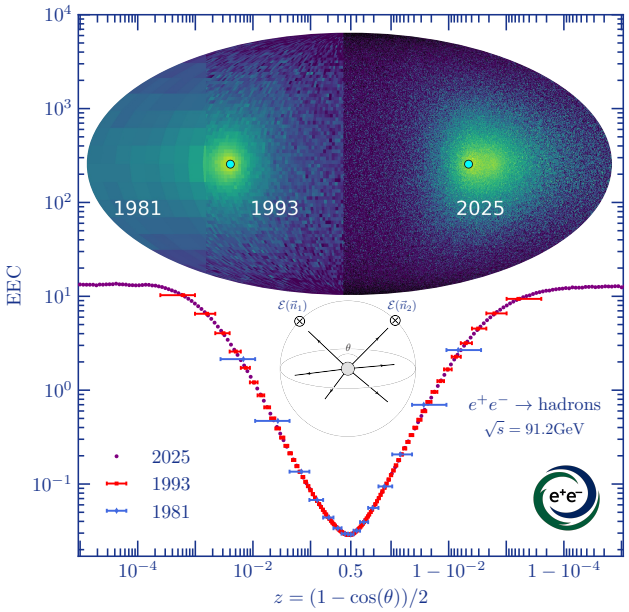

Fig. 1: The energy flux in e^+e^- collisions, and the corresponding EEC distribution, illustrating 45 years of experimental efforts and developments: the first PLUTO measurement (1981), LEP measurements with hadronic calorimeters (1993), and the track based ALEPH measurement (2025). The two energy flow operators are illustrated as green dots. Varying angles, one probes physics at different scales estimated by $Q\min[\sqrt{z}, \sqrt{1-z}]$, exhibiting different scaling laws. The $z \to 0$ limit is controlled by collinear physics and the distribution scales as $z^{-1+\gamma^{(3)}}$, whereas the $z \to 1$ limit probes the conventional TMD regime. The apparent symmetry of the distribution is therefore accidental. Figure reproduced from [13].

The back-to-back endpoint also involves a transition, but of a different kind. For $z \to 1$, the dynamics are instead those of a recoil-sensitive TMD observable governed together by soft and collinear radiations, and the appropriate variable is the recoil away from perfect momentum balance. In this region, it is useful to trade the angular variable for a recoil momentum [23],

$$\frac{d\Sigma}{dz} = \frac{1}{2\sigma}\sum_{i,j}\int dx_i\, dx_j\, x_i x_j\, \frac{d^3\sigma}{dx_i\, dx_j\, dz}, \tag{5}$$

with

$$\frac{d^3\sigma}{dx_i\, dx_j\, dz} = \int d^2\vec{k}_\perp\, \frac{d^3\sigma}{dx_i\, dx_j\, d^2\vec{k}_\perp}\,\delta\!\left(1 - z - \frac{\vec{k}_\perp^{\,2}}{Q^2}\right). \tag{6}$$

Here x_i and x_j are the energy fractions of the measured particles, and $\vec{k}_\perp$ is the net recoil transverse momentum, which vanishes in the exact back-to-back limit. Equation (6) shows that the distance from $z = 1$ is set by $k_\perp^2/Q^2$, placing the back-to-back EEC in the same recoil-sensitive class as standard TMD factorization observables [21, 23].

The standard EEC thus contains a recoil-sensitive back-to-back TMD region and a small-angle limit with perturbative, transition, and post-confinement domains, making it a versatile tool for exploring hadron structure and a broad range of hadronic dynamics.

2.1.2 Back-to-back EEC: the TMD dynamics

In the back-to-back limit, $1 - z \sim k_\perp^2/Q^2 \ll 1$, the differential cross section factorizes at leading power as [23]

$$\left.\frac{d^3\sigma}{dx_i\, dx_j\, dz}\right|_{z\to 1} = \frac{1}{2}H(Q,\mu)\int d^2\vec{k}_\perp \int \frac{d^2\vec{b}_\perp}{(2\pi)^2} e^{-i\vec{b}_\perp\cdot\vec{k}_\perp}\,\delta\!\left(1 - z - \frac{\vec{k}_\perp^{\,2}}{Q^2}\right) F_{q\to i}\!\left(x_i, \frac{\vec{b}_\perp}{x_i}, \mu, \nu\right) F_{q\to j}\!\left(x_j, \frac{\vec{b}_\perp}{x_j}, \mu, \nu\right) S_{\rm EEC}(\vec{b}_\perp, \mu, \nu)\,. \tag{7}$$

Here x_i and x_j are the energy fractions of the two measured hadrons, $\vec{k}_\perp$ is the total imbalance conjugate to $1 - z$. The scales μ and ν denote the renormalization and rapidity scales, respectively. The hard function $H(Q,\mu)$ governs the short-distance production, the TMD fragmentation functions $F_{q\to i}$ and $F_{q\to j}$ describe the two collinear jets, and the soft function $S_{\rm EEC}$ carries the recoil-sensitive rapidity dynamics. At leading power, the back-to-back EEC is therefore a recoil-sensitive TMD observable.

The corresponding soft sector admits the operator definition [23]

$$S_{\rm EEC}(\vec{b}_\perp, \mu, \nu) = \lim_{\nu\to+\infty}\frac{1}{N_c}\mathrm{tr}\,\langle 0|\,T\Big[S^\dagger_{\bar{n}+}(0)S_{n-}(0)\Big]\,\bar{T}\Big[S^\dagger_{n+}(y_\nu(\vec{b}_\perp))S_{\bar{n}-}(y_\nu(\vec{b}_\perp))\Big]\,|0\rangle\,. \tag{8}$$

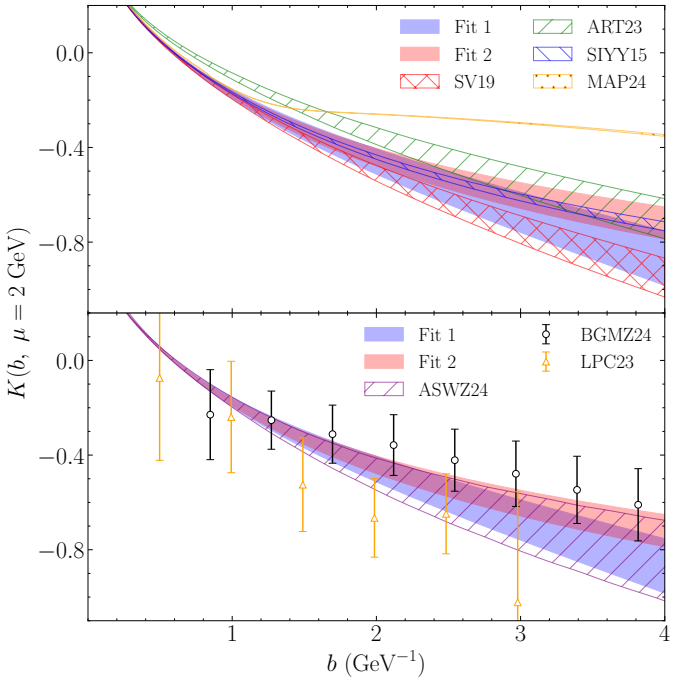

Fig. 2: The comparison of the full Collins-Soper kernel $K(b, \mu = 2\text{GeV})$ extracted from EEC in Ref. [74] with other phenomenological extractions in [76–79] in the upper plot, and to lattice QCD calculations from different collaborations [80–82] in the lower panel. Figure from Ref. [74].

Here

$$y_\nu(\vec{b}_\perp) = \left(\frac{ib_0}{\nu}, \frac{ib_0}{\nu}, \vec{b}_\perp\right), \qquad b_0 = 2e^{-\gamma_E}, \tag{9}$$

and the vectors n and $\bar{n}$ are the two lightlike jet directions, $\vec{b}_\perp$ is the impact parameter conjugate to the recoil momentum, and $S_{n\pm}$ and $S_{\bar{n}\pm}$ are eikonal Wilson lines. The rapidity-regulated shift $y_\nu(\vec{b}_\perp)$ defines the soft matrix element whose rapidity evolution enters the Collins-Soper structure. Its relation to the standard DIS/TMD soft sector is [33]

$$S_{n\bar{n}}(b_\perp, \mu, \nu) = S_{\mathrm{EEC}}\left(b_\perp,\ L_\nu + \ln\frac{n\cdot\bar{n}}{2},\ \mu\right), \tag{10}$$

with $b_\perp = |\vec{b}_\perp|$ and L_ν the rapidity logarithm. The same rapidity-sensitive soft physics therefore appears in both the back-to-back EEC and DIS TMD factorization, so that the back-to-back EEC is governed by the same Collins-Soper rapidity evolution that controls TMD observables [3, 33, 74, 75].

After summing over hadrons with the energy weight, the EEC jet function obeys the sum rule [33]

$$J_f(b_\perp, E_{\bar{n}}, \mu, \nu) \equiv \sum_h \int_0^1 dx\, x\, F^{\mathrm{OPE}}_{h/f}\left(x, \frac{b_\perp}{x}, E_{\bar{n}}, \mu, \nu\right) = \sum_i \int_0^1 d\xi\, \xi\, C_{if}\left(\xi, \frac{b_\perp}{\xi}, E_{\bar{n}}, \mu, \nu\right), \tag{11}$$

where J_f is the flavor-f EEC jet function, $E_{\bar{n}}$ is the energy flowing into the $\bar{n}$-collinear jet, $F^{\mathrm{OPE}}_{h/f}$ is the OPE-matched TMD fragmentation function into hadron h, and C_{if} are the perturbative matching coefficients. The hadronic and partonic fragmentation fractions are denoted by x and ξ, respectively. After the energy-weighted sum, the back-to-back EEC is expressed in terms of the same matching coefficients that appear in TMD fragmentation, with the replacement of the conventional TMD fragmentation function by the EEC jet function.

$$\frac{d\Sigma}{dz}\Big|_{z\to 1} = \frac{1}{2\sigma} H(Q,\mu) \int d^2\vec{k}_\perp \int \frac{d^2\vec{b}_\perp}{(2\pi)^2} e^{-i\vec{b}_\perp\cdot\vec{k}_\perp} \delta\left(1 - z - \frac{\vec{k}_\perp^2}{Q^2}\right) J_f\left(\vec{b}_\perp, E_n, \mu, \nu\right) J_{\bar{f}}\left(\vec{b}_\perp, E_{\bar{n}}, \mu, \nu\right) S_{\mathrm{EEC}}(\vec{b}_\perp, \mu, \nu)\,. \tag{12}$$

The back-to-back EEC therefore probes the same recoil-sensitive dynamics that underlie conventional back-to-back hadron and jet observables, with the identified object replaced by an energy-weighted flow measurement. The factorization theorem for projected N-point energy correlators in the back-to-back limit has also been discussed recently [64].

The same logic extends beyond the unpolarized e^+e^- case. In spin-dependent DIS, the energy-weighted correlator in the current-fragmentation, nearly back-to-back region takes the form [33]

$$y\,\frac{d\sigma^{\rm EC}_{\ell+N\to\ell'+X}}{d^2\vec{q}_\perp\,dx\,dy} \simeq \sum_f \int \frac{d^2\vec{b}_\perp}{(2\pi)^2} e^{i\vec{b}_\perp\cdot\vec{q}_\perp} \Big[H_f(Q^2,\mu) S_{n\bar{n}}(b_\perp,\mu,\nu)\Big] J_f(b_\perp,E_{\bar{n}},\mu,\nu) \Big[\sigma_0^U\, xB_{f/N}(x,b_\perp,E_n,\mu,\nu) + \lambda_\ell S_\parallel\, \sigma_0^L\, x\Delta B_{f/N}(x,b_\perp,E_n,\mu,\nu)\Big]. \quad (13)$$

Here x and y are the DIS Bjorken and inelasticity variables, $\vec{q}_\perp$ is the measured transverse recoil, E_n and $E_{\bar{n}}$ are the characteristic energies along the beam and current directions, λ_ℓ is the lepton helicity, and $S_\parallel$ is the longitudinal target polarization. The functions $B_{f/N}$ and $\Delta B_{f/N}$ are the unpolarized and polarized TMD beam functions, while $\sigma_0^{U,L}$ are the corresponding leptonic prefactors. The back-to-back energy correlator in DIS is governed by the same EEC jet function and the same soft sector as in the standard problem; the spin dependence enters through the polarized beam function $\Delta B_{f/N}$ [33]. Collins-type azimuthally dependent correlators have also been proposed as probes of nucleon structure and TMD dynamics in SIDIS-like settings [70]. Back-to-back TEECs in ep collisions probe small-x spin structure; in this case the Sivers asymmetry can be related to C-odd odderon exchange within TMD factorization [52].

In e^+e^- annihilation, the precision frontier for Eq. (11) is at next-to-next-to-next-to-next-to leading logarithmic ($\mathrm{N^4LL}$) resummation accuracy and is further matched onto the next-to-next-to-leading-order (NNLO) fixed order calculation [20]. An additional but very good approximation is required in the fixed order prediction for the EEC measured using tracks [20], since the energy correlator measured on tracks is not infrared-collinear (IRC) safe. The $\mathrm{N^3LL}$ resummation was also achieved for back-to-back TEEC in pp collisions [48, 51] and the current fragmentation region EC in DIS of Eq. (13) [33].

This level of perturbative control opens the possibility of using the back-to-back EEC as a precision probe of TMD dynamics. For phenomenology, however, the strictly asymptotic endpoint description is not sufficient. At the level of present precision, the large-$b_\perp$ behavior of the rapidity evolution, conventionally encoded in the nonperturbative part of the Collins-Soper kernel, can become numerically relevant together with other nonperturbative corrections [20]. This has motivated a recent precision program based on comparisons between resummed EEC predictions and e^+e^- data [20, 75, 83, 84].

Ref. [83] treated the back-to-back EEC as jointly sensitive to $\alpha_s(m_Z)$ and to the nonperturbative component of rapidity evolution, and performed a simultaneous extraction at $\mathrm{N^3LL}$ accuracy. The resulting comparison with other phenomenological and lattice determinations of the Collins-Soper kernel is shown in Fig. 2. Working at $\mathrm{N^4LL}$ accuracy, Ref. [75] examines the same strategy, arguing that existing data provide only limited constraining power on the kernel. Ref [75] further suggests that the situation could be improved by data from ongoing or future experiments, such as Belle II, by which 5% precision measurement will improve constraints on the Collins-Soper kernel. We note that both the analyses are based on e^+e^- data that did not exploit the superior angular resolution of track-based measurements. An analysis using the corresponding e^+e^- benchmark provided by the archived ALEPH Z-pole study at 91.2 GeV [13], which brings the back-to-back EEC into direct contact with modern source-unfolded data, is therefore well motivated. An extraction that includes the recent ALEPH datasets was carried out in Ref. [84] which combines $\mathrm{N^3LL}$ resummation in the back-to-back region with NNLO fixed-order calculations.

2.1.3 Small-angle EEC: hadronization, di-hadron fragmentation and light-ray OPE

In the small-angle limit, $z \to 0$, the distribution is governed by the leading-power factorization theorem [8, 9]

$$\frac{d\Sigma}{dz}\Big|_{z\to 0} = \frac{1}{\sigma}\sum_a \int_0^1 d\xi\,\xi^2\; j_a\left(z\xi^2Q^2,\mu^2,\Lambda^2_{\rm QCD}\right) H_a\left(\xi,\ln\frac{Q^2}{\mu^2}\right), \quad (14)$$

where H_a denotes the hard function for producing a parton a carrying momentum fraction ξ. Unlike the jet function that appears in the back-to-back limit, the jet function j_a in this regime depends on both energy insertions. The form of this factorization theorem is fixed by Lorentz symmetry, renormalization-group invariance, and the general structure of the EEC in massless QCD [9], and it remains valid throughout the perturbative, transition, and post-confinement regimes. Both the hard and jet functions obey DGLAP-like evolution equations.

In the perturbative region $Q \gg Q\sqrt{z} \gg \Lambda_{\rm QCD}$, the leading power jet function is independent of $\Lambda_{\rm QCD}$ and is known perturbatively at NNLL accuracy. It predicts the scaling law, $d\Sigma/dz \sim z^{-1+\gamma(3)}$ visible for example in Fig. 1 and Fig. 4. Here, $\gamma(3)$ is the 3rd moment of the singlet splitting function (twist-2 spin-3 anomalous dimension) [2]. The scaling law was first derived in the framework of CFT [6]. Phenomenologically, the scaling law in this region was used as a determination of the strong coupling constant by the CMS collaboration [28]. By taking the ratio of E3C/EEC in jets at the LHC with $\sqrt{s} = 13$ TeV, CMS measures $\alpha_S(M_Z) = 0.1229^{+0.0040}_{-0.0050}$ which sets the most precise $\alpha_S(M_Z)$ value obtained using jet substructure observables.

In the perturbative regime, the leading nonperturbative power correction to Eq. (14), of order $\Lambda_{\rm QCD}/Q$, was derived in Ref. [85] by analyzing the leading renormalon ambiguity of the EEC in e^+e^- annihilation. It takes the form

$$\frac{d\Sigma^{NP}}{dz}\Big|_{z\to 0} = \frac{1}{2}\,\frac{\Omega_{1,q}}{Q[z(1-z)]^{3/2}}, \quad (15)$$

where

$$\Omega_{1,i} = \frac{1}{N_i}\langle\Omega|Y_nY^\dagger_{\bar{n}}\mathcal{E}_T(0)Y_{\bar{n}}Y^\dagger_n|\Omega\rangle \quad (16)$$

[2] More precisely its eigenvalues, since it involves multiple such operators.

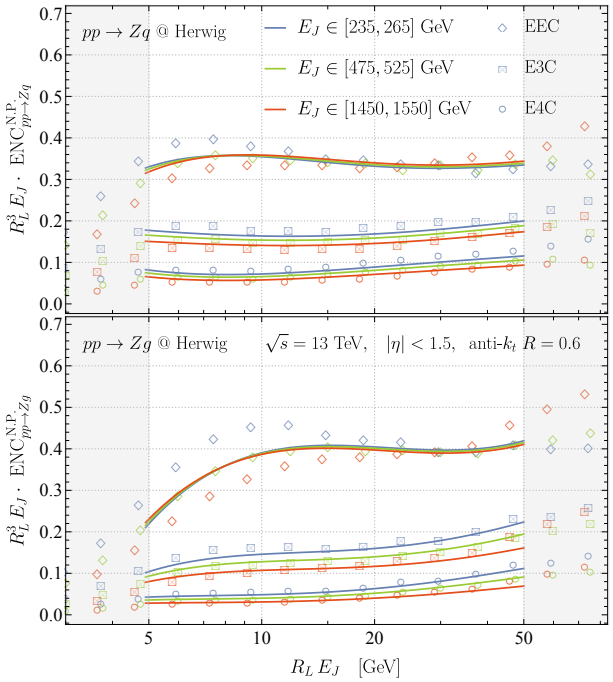

Fig. 3: Quantum scaling of the leading non-perturbative power correction for ENC in the perturbative small angle region. Here $E_J \sim Q$ and $R_L \sim \chi \sim \sqrt{z}$. Figure from [92].

	$\mathcal{E}$	$\mathcal{E}\mathcal{E}$	$\vec{\mathbb{O}}_\tau^{[J]}$	z	Λ_{QCD}, Q
J_L	-3	-6	$1-(\tau+J)$	2	0
$-\Delta_L$	1	2	$J-1$	0	1

Table 1: Light-ray spin (boost) and scaling dimension of various quantities used in OPE.

is the same leading power correction that appears in e^+e^- event-shape observables in the dijet limit [86–90]. Here $N_q = N_C$, $N_g = N_C^2 - 1$, and $\mathcal{E}_T(\eta) = \frac{1}{\cosh^3\eta}\int d\phi\, \mathcal{E}(\vec{n}) = (2z(1-z))^{3/2}\int d\phi\, \mathcal{E}(\vec{n})$ denotes the transverse energy-flow operator. The specific form of $\Omega_{1,i}$ in Eq. (16) follows from boost invariance.

This leading-power analysis admits a simple physical interpretation. At lowest order in α_s, the leading Λ_{QCD}/Q correction arises when one of the energy-flow detectors is aligned with soft hadrons with energies of order Λ_{QCD}, while the other is aligned with one of the energetic dijets. Ref. [91] further generalized this result to N-projected point energy correlators in e^+e^- and showed that, for any N, the leading correction is governed by the same universal parameter $\Omega_{1,i}$.

A complementary perspective on the nonperturbative corrections was developed in Ref. [92], which uses light-ray operator product expansion (OPE) techniques to organize power corrections without assuming an explicit operator form for the correction. For the simplest two-point energy correlator, the light-ray OPE at leading twist, $\tau = 2$, reads

$$\lim_{n_1\to n_2}\mathcal{E}(n_1)\mathcal{E}(n_2) = \frac{1}{z}\vec{C}(\mu)\cdot\vec{\mathbb{O}}^{[J=3]}_{\tau=2}(n_2,\mu) + \frac{\Lambda_{\mathrm{QCD}}}{z^{3/2}}\vec{D}(\mu)\cdot\vec{\mathbb{O}}^{[J=2]}_{\tau=2}(n_2,\mu) + \cdots, \tag{17}$$

where $\vec{C}$ and $\vec{D}$ are OPE coefficients related to the jet function j_a, and the twist-2 light-ray operators, also known as the DGLAP operators [93], are

$$\vec{\mathbb{O}}^{[J]}_{\tau=2} = \mathbb{L}_2[\vec{O}^{[J]}_{\tau=2}],\quad \vec{O}^{[J]}_{\tau=2} = \begin{pmatrix} \frac{1}{2^J}\bar{\psi}\gamma^+(iD^+)^{J-1}\psi \\ \frac{-1}{2^J}G^{a,\mu+}(iD^+)^{J-2}G^{a,+}_\mu \end{pmatrix}, \tag{18}$$

Here $\mathbb{L}_\tau = \lim_{r\to\infty} r^\tau \int_0^\infty dt$ denotes the light-ray transform. The light-ray operators are characterized by the light-ray dimension $-\Delta_L = J-1$ and the light-ray spin $J_L = -\Delta + 1$, where J and Δ are the spin and scaling dimension of the local operator O prior to the light-ray transform. In the light-ray OPE, the light-ray dimension $-\Delta_L = J-1$ and spin $J_L = -\Delta+1$ must match on both sides of Eq. (17). For twist operators, $\Delta - J = \Delta_L - J_L = \tau$, and therefore $J = -\Delta_L + 1 = -J_L - \tau + 1$. Table 1 summarizes quantities that appear frequently in analyses of the light-ray OPE for energy correlators. A similar light-ray OPE strategy also applies to N-projected point energy correlators.

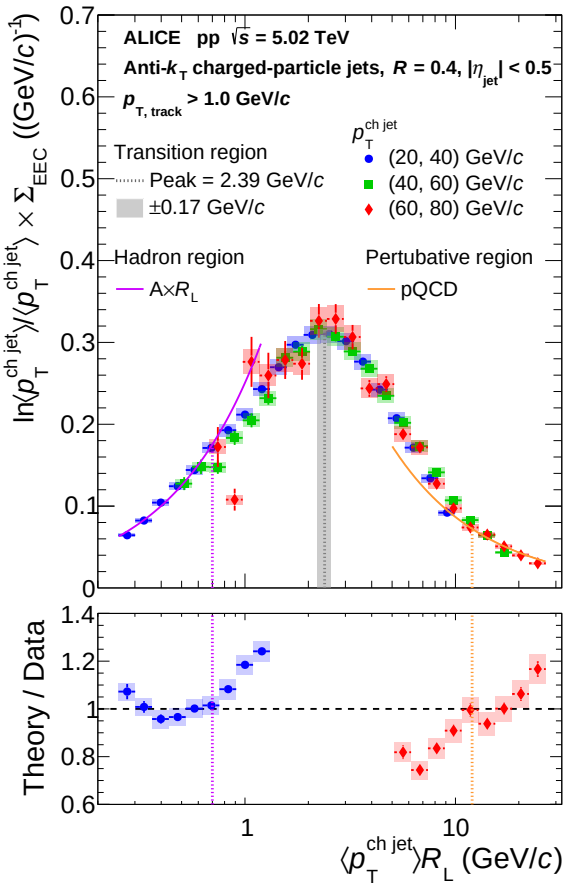

Fig. 4: Observed parton to hadron transition scales in jets by ALICE [11]. Here $R_L \sim \chi \sim \sqrt{z}$ and $Q \sim \langle p_T^{\text{ch jet}} \rangle$. Left to the shaded transition region locates the post-confinement domain. The shape difference in the post-confinement domain between this measurement and the LEP data in Fig. 1 is due to the variable change $\frac{1}{Q}\frac{d\Sigma}{d\ln Q\chi} = \frac{\chi}{2}\frac{d\Sigma}{Q^2 dz}$, which transforms the plateau behavior seen in $\frac{d\Sigma}{dz}$ to the sloped line in $\frac{1}{Q}\frac{d\Sigma}{d\ln Q\chi}$. Figure reproduced from [11]

The twist-2 light-ray operator $\vec{\mathbb{O}}^{[J]}_{\tau=2}(n,\mu)$ obeys the DGLAP evolution equation [7, 9, 94, 95]

$$\mu\frac{d}{d\mu}\vec{\mathbb{O}}^{[J]}_{\tau=2}(n;\mu) = \gamma^{[J]}_{\tau=2}(\mu)\cdot\vec{\mathbb{O}}^{[J]}_{\tau=2}(n;\mu)\,, \tag{19}$$

where $\gamma^{[J]}_{\tau=2}$ is the anomalous-dimension matrix for the twist-2 light-ray operators and is given exactly by the J-th Mellin moment of the splitting function. Renormalization-group invariance then implies the quantum scaling of the EEC power correction, yielding

$$\frac{d\Sigma^{NP}}{dz}\Big|_{z\to 0} = z^{-3/2}\frac{\Lambda_{\text{QCD}}}{Q}\vec{D}\left(1,\frac{\Lambda^2_{\text{QCD}}}{\mu_J^2}\right)\cdot U(\mu_J,Q)\cdot\frac{\langle\vec{\mathbb{O}}^{[J=2]}_{\tau=2}(n;Q)\rangle}{(4\pi)^{-1}\sigma Q}\,, \tag{20}$$

where $U(\mu_J, Q)$ is the evolution operator

$$U(\mu_J,Q) \equiv \mathbb{P}\exp\left(-\int_{\mu_J}^{Q}\frac{d\mu}{\mu}\gamma^{[J=2]}_{\tau=2}(\mu)\right). \tag{21}$$

and $\mu_J \sim Q\sqrt{z}$ is the natural scale for the OPE coefficient $\vec{D}$ or the jet function j_a. Given the power correction at a scale Q_0, Eq. (20) predicts its value at another scale Q. Since $\langle\vec{\mathbb{O}}^{[J=2]}_{\tau=2}(n;Q)\rangle \sim Q$, as seen from Eq. (18), the combination $Qz^{3/2}d\Sigma^{NP}/dz$ is independent of Q up to logarithmic evolution. Such predictions are presented in Fig. 3 for energy correlators measured in $pp \to Zq$ and $pp \to Zg$ using Herwig simulation. Recently, the light-ray OPE was also applied to analyze the EEC power correction and its scaling at generic angles [96]. Through detector matching [93], the resulting anomalous dimension is related to the BFKL detector eigenvalue, tying the scaling of energy-flow power corrections to Regge light-ray dynamics.

As z decreases, the EEC undergoes a transition from the perturbative to the nonperturbative domain, with distinct scaling behaviors observed experimentally [12]. A plateau emerges in the post-confinement region $Q\sqrt{z} \lesssim \Lambda_{\rm QCD}$, suggesting an approximately uniform distribution of hadrons in this regime. Figure 4 shows the ALICE measurement of the EEC distribution in jets using charged hadrons. The presentation adopted by the ALICE collaboration is equivalent to an additional normalization of the EEC by the squared jet energy $Q^2 \sim \langle p_T^{\rm ch\ jet}\rangle^2$. As seen in Fig. 4, in the post-confinement domain, this further Q^2-normalized-EEC is approximately independent of the input energy Q, up to mild $\ln Q$ corrections. Although the plateau itself is qualitatively consistent with several strong-coupling-inspired model predictions [6], the observed Q^2 scaling is hard to accommodate, since most such models predict Q-independent EEC in the post-confinement domain and hence a Q^{-2} behavior for EEC$/Q^2$. For a long time, the nonperturbative regime remained much less understood.

Since the EEC is dimensionless, its approximate Q^2 scaling points to the presence of an intrinsic scale that compensates the dimensionality. A purely conformal description does not by itself supply such a dimensionful scale. In QCD, by contrast, the natural candidate is $\Lambda_{\rm QCD}$ which implies that in the post-confinement regime one expects $d\Sigma/dz \sim Q^2/\Lambda_{\rm QCD}^2$. The appearance of the factor $\Lambda_{\rm QCD}^{-2}$ in turn suggests the existence of a nonperturbative distribution that controls the dynamics in the post-confinement region. Indeed, recent studies [15–19] uncovered the di-hadron fragmentation nature of this region, which show that jet function j_a in the factorization theorem in Eq. (14) is related to the di-hadron fragmentation function (DiFF) by

$$j_a(z\xi^2Q^2,\mu^2,\Lambda_{\rm QCD}^2) = \sum_{h_1,h_2}\int dw_1\,dw_2\,d^2\vec{R}_T\,\delta\!\left(z-\frac{\vec{R}_T^2}{\xi^2Q^2}\frac{1}{w_1^2w_2^2}\right) w_1w_2\,\mathcal{D}^{h_1h_2/a}(w_1,w_2,\vec{R}_T,\mu^2)\,, \tag{22}$$

where $\mathcal{D}^{h_1h_2/a}$ is the unpolarized diFF for parton $a\to h_1h_2$. $\vec{R}_T$ is the relative transverse momentum of h_1 and h_2. ξ is the parton momentum fraction and $w_{1/2}$ is the hadron momentum fraction with respect to the fragmenting parton.

One can further expand in z (or equivalently $\vec{R}_T$) to find [16]

$$j_a(z\xi^2Q^2,\mu^2,\Lambda_{\rm QCD}^2)|_{z\to0} = \xi^2Q^2\sum_{h_1,h_2}\int dw_1\,dw_2\;w_1^2w_2^2\,\mathcal{D}^{h_1h_2/a}(w_1,w_2,\vec{0},\mu^2)+\dots\,, \tag{23}$$

where $\dots$ represents terms suppressed as $z\to0$. Plugging the expanded the jet function back into Eq. (14), one finds

$$\frac{d\Sigma}{dz} = Q^2\left[\sum_{h_1,h_2}\int dw_1\,dw_2\;w_1^2w_2^2\,\mathcal{D}^{h_1h_2/a}(w_1,w_2,\vec{0},\mu^2)\right]\times\left[\frac{1}{\sigma}\int d\xi\xi^4H_a\left(\xi,\ln\frac{Q^2}{\mu^2}\right)\right]+O(z) \tag{24}$$

which predicts the Q^2 scaling in the post-confinement domain. The corresponding quantum scaling follows from the evolution of the DiFF $\mathcal{D}^{h_1h_2/a}$ and the inclusive single-parton production cross section H_a.

The same post-confinement scaling can also be derived from the light-ray OPE without assuming the DiFF representation [16]. Matching the light-ray dimension and spin, and considering the post-confinement plateau behavior, gives the leading contribution [16]

$$\lim_{n_1\to n_2}\frac{\langle\mathcal{E}(n_1)\mathcal{E}(n_2)\rangle}{Q^2} = Q^2z^0\left[\frac{\vec{\mathcal{D}}(\mu)}{\Lambda_{\rm QCD}^2}\right]\cdot\frac{\langle\vec{\mathbb{O}}_{\tau=2}^{[J=5]}(n_2,\mu)\rangle}{Q^4}+O(z,Q\Lambda_{\rm QCD}^{-1})\,, \tag{25}$$

since $\mathcal{E}\mathcal{E}$ with $J_L=-6$ and $-\Delta_L=2$, together with the z^0 scaling, fixes $J=5$ for twist-2 operators and determines the $\Lambda_{\rm QCD}^{-2}$ coefficient. Ref. [16] also extended the light-ray OPE analysis to power-suppressed terms in z and to nonlinear powers of the energy-flow operator $\mathcal{E}^m$.

Recalling that $\langle\vec{\mathbb{O}}_{\tau=2}^{[J=5]}(n_2,\mu)\rangle$ scales as Q^4, as indicated by Eq. (18), the light-ray OPE analysis recovers the Q^2 scaling in the post-confinement domain. Furthermore, since $\langle\vec{\mathbb{O}}_{\tau=2}^{[J=5]}(n_2,\mu)\rangle/Q^4$ is simply the fourth moment of the single-parton production rate, one can identify the OPE coefficient $\frac{\vec{\mathcal{D}}(\mu)}{\Lambda_{\rm QCD}^2}$ with the corresponding moment of the DiFF in Eq. (24) [16].

Repeating the previous derivation with the replacement $J=2\to J=5$, one finds that the EEC in the post-confinement region is given by

$$\frac{d\Sigma^{P.C.}}{dz}\Big|_{z\to0} = \frac{Q^2}{\Lambda_{\rm QCD}^2}\vec{\mathcal{D}}(\mu_J/\Lambda_{\rm QCD})\cdot U(\mu_J,Q)\cdot\frac{\langle\vec{\mathbb{O}}_{\tau=2}^{[J=5]}(n;Q)\rangle}{(4\pi)^{-1}\sigma Q^4}\,, \tag{26}$$

where $U(\mu_J,Q)$ is the evolution operator

$$U(\mu_J,Q)\equiv\mathbb{P}\exp\left(-\int_{\mu_J}^{Q}\frac{d\mu}{\mu}\gamma_{\tau=2}^{[J=5]}(\mu)\right). \tag{27}$$

Therefore, once the height of the post-confinement plateau is known at one energy scale Q_0, its height at a different energy Q can be predicted from Eq. (26).

Beyond its connection to DiFFs, Ref. [16] proposed using the quantum scaling of the post-confinement plateau height to determine α_s, with controlled nonperturbative inputs ($\mathcal{D}_g$ and $\mathcal{D}_q$). Although the current theoretical control is limited to LL/NLL accuracy, this framework could be extended to NNLL resummation matched to N^{3}LO fixed-order results in e^+e^- [97] and ep [98] collisions, as well as to N^{2}LO at the LHC [99], by adapting calculations that are already available. Further progress on the four-loop splitting functions [100] could, once completed, push the resummation accuracy to N^{3}LL.

The transverse-spin sector of the light-ray OPE was applied to the squeezed limit of the three-point energy correlator [95]. In this limit, the QCD light-ray OPE shows that the leading-twist expansion of energy-flow operators closes onto light-ray operators with transverse spin

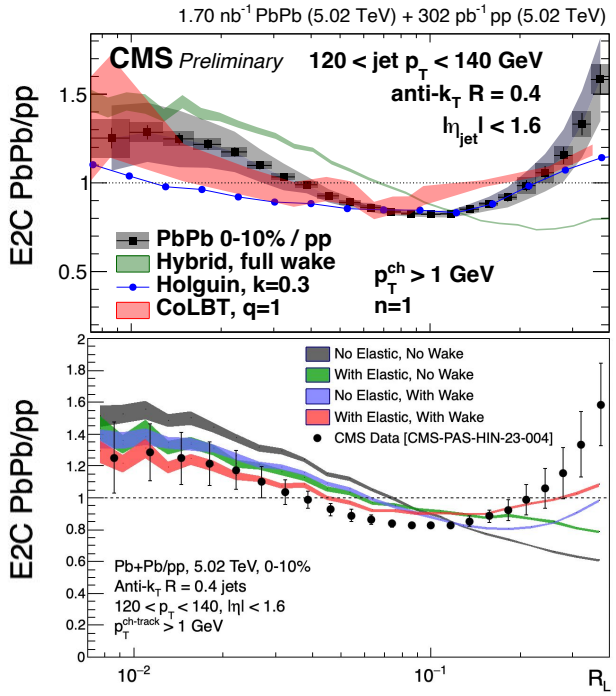

Fig. 5: Ratio of the EEC in Pb-Pb and p-p collisions compared with representative theoretical calculations. The measured shape contains both genuine medium modification and the bias induced by selecting quenched jets at fixed reconstructed energy. Figure from Ref. [106].

$j = 0, 2$, so that the transverse-spin-two gluon operator provides a natural $\cos(2\phi)$ analyzer of spinning gluons. This observation underlies later EEC-based proposals for gluon polarimetry [42, 101]

2.1.4 Energy correlators for hot and cold nuclear matter

Energy correlators measure how the angular pattern of a jet is modified by matter. Different components of the in-medium shower populate different angular regions. The small-angle region remains tied to collinear evolution and hadronization, while larger angles are sensitive to the scale at which the medium resolves and redistributes the jet energy. In heavy-ion collisions this separation is nontrivial, since perturbative radiation, elastic scattering, recoil, hydrodynamic response, transport, and hadronization all contribute to the measured distribution. For broader reviews of jet quenching and jet substructure in nuclear collisions, see Refs. [102–105]. The basic nuclear observable is the ratio to a proton baseline,

$$R_{AA}^{\mathrm{EEC}}(\theta) = \frac{d\Sigma_{AA}/d\theta}{d\Sigma_{pp}/d\theta}, \qquad R_{pA}^{\mathrm{EEC}}(\theta) = \frac{d\Sigma_{pA}/d\theta}{d\Sigma_{pp}/d\theta}, \tag{28}$$

with the jet definition, kinematic cuts, and energy weighting kept fixed between numerator and denominator. The first CMS measurement of energy correlators inside high-p_T jets in Pb-Pb collisions observed a significant modification relative to the p-p reference [106]. At fixed reconstructed jet energy, the ratio receives contributions from both large-angle medium response and quenching bias. The selected Pb-Pb jets originate from a different distribution of initial parton energies and from a shifted quark-gluon composition. This bias can affect the transition and hadronization regions before the genuine medium response is isolated.

The first theoretical interpretations separate into two closely related directions. One treats the EEC as a perturbative probe of the angular structure of medium-induced radiation. The semi-hard implementation of the BDMPS-Z multiple-scattering formalism [107–112] was used by Andres, Dominguez, Holguin, Marquet, Moult, and collaborators to identify the angular scale at which the QGP resolves the jet and to quantify how quenching bias enters inclusive-jet comparisons [24, 26, 113–116]. A second direction follows the full jet and its recoil through the medium. The CoLBT calculation of Yang, He, Moult, and Wang combines coupled Boltzmann transport [117–119], the linear Boltzmann transport framework [120–123], high-twist energy loss [124, 125], CLVisc hydrodynamics [126–128], and hybrid hadronization [129, 130]. In this description the large-angle enhancement is dominated by medium response from elastic scatterings, whereas the small-angle suppression reflects parton energy loss and transverse-momentum broadening [131]. Together these calculations show that the EEC is sensitive not only to the amount of energy loss, but also to the angular scale at which the medium resolves and redistributes the jet energy.

Flavor composition provides an additional handle on this physics. Heavy-flavor jets contain the dead-cone scale $\theta_m \sim m_Q/p_T$, below which vacuum radiation from a heavy quark is suppressed [132]. Medium-induced radiation and elastic scattering can partially populate this region, so that the dead-cone scale and the medium-modification scale are separated at sufficiently large jet energy and become entangled

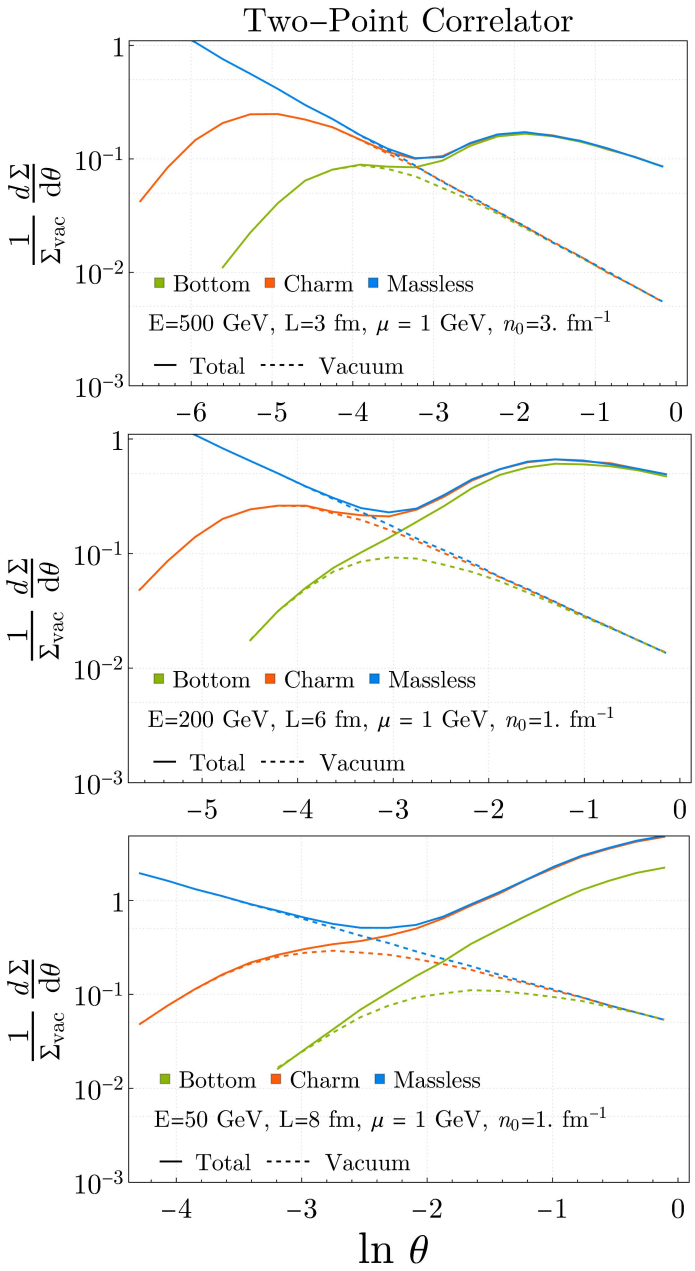

Fig. 6: EEC for heavy-quark jets in a QGP. At high energy the dead-cone and medium-modification scales are separated; at lower energy the medium fills the dead cone. Figure reproduced from Ref. [114].

at lower energy [114, 133, 134]. Xing, Cao, Qin, and Wang studied heavy- and light-flavor jet EECs in a realistic QGP simulation and found a clear flavor hierarchy, controlled by the interplay of quark mass, parton energy loss, induced radiation, and medium response [135]. Flavor selection also changes the quark-gluon mixture of inclusive and photon-tagged jet samples, which can generate visible modifications of the EEC ratio even before one isolates the microscopic origin of the medium response [136]. The first ALICE measurement of EECs in charm-tagged jets in p-p collisions provides the corresponding experimental benchmark for this flavor-differential program [137].

The separation of medium response from selection bias can be sharpened by exploiting the approximate scaling of the small-angle correlator. Refs. [115, 116] introduced an unbiasing transformation that removes the leading effect of the shifted initiating parton energy. After this transformation, the centrality dependence of the large-angle enhancement becomes clearer: it is largest in central Pb-Pb events and decreases toward peripheral collisions. This behavior supports a medium-origin interpretation of the large-angle modification, while leaving residual flavor-composition and jet-selection effects to be controlled in precision comparisons. Color-neutral tagged samples, such as photon- or Z-recoiling jets, provide a complementary way to reduce the same ambiguity.

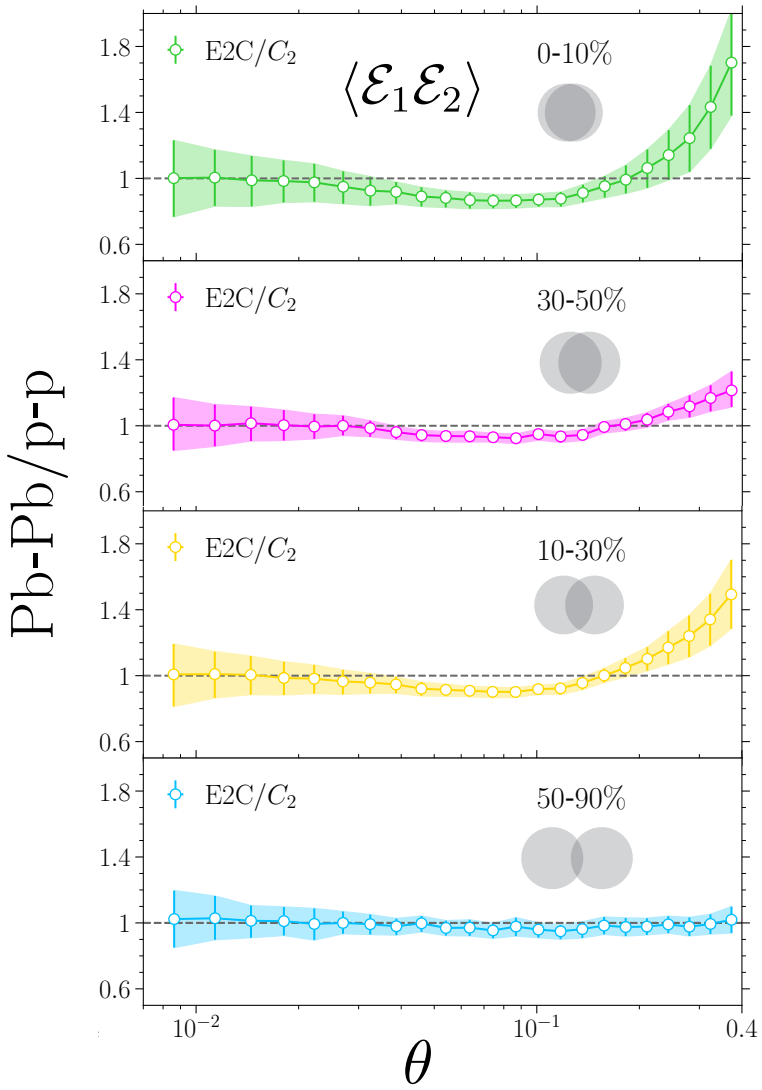

Fig. 7: Unbiased ratio of the EEC in Pb-Pb and p-p collisions as a function of centrality. The reduction of the enhancement from central to peripheral collisions supports a medium-response interpretation of the large-angle modification. Figure adapted from Refs. [115, 116].

The two-point correlator locates the angular scale of nuclear modification. Higher-point correlators probe the geometry of the radiation at that scale. In the hybrid strong/weak-coupling model, the first shape-dependent three-point study showed that configurations with three well-separated detector directions are especially sensitive to hadrons produced by the wake excited by the jet in the QGP [138]. A later two- and three-point analysis in the same phenomenological framework included elastic scattering and wakes sourced by recoiling partons, improving the comparison with CMS and ALICE measurements and motivating correlator variants with enhanced wake sensitivity [139]. The hydrodynamic response has also been treated analytically for the energy flux and the two-point EEC; in that case the medium back-reaction produces a large-angle contribution that competes with the perturbative QCD component [140]. Barata, Moult, Sadofyev, and Silva then developed a systematic multi-point treatment of jets fragmenting in a dense QGP, showing how projected N-point correlators and shape-dependent three-point correlators distinguish perturbative modification of the cascade from hydrodynamic back-reaction [141]. A further step was taken in Ref. [142], where the EEC was studied directly on many-body QCD states rather than only on jets propagating through a medium. In a near-equilibrium state, the small-angle correlator is organized into several dynamical regimes. At the largest separations within the small-angle region, the disconnected contribution is fixed by the collective flow of the medium and gives a classical hydrodynamic scaling. At smaller separations, connected stress-tensor fluctuations become important and the correlator is controlled by hydrodynamic modes. At still smaller angles, the hydrodynamic description must be matched onto the light-ray OPE, before the observable eventually reaches the dilute hadronic regime. The explicit construction with boost-invariant Gubser flow shows how collective geometry and azimuthal perturbations are imprinted directly on the final-state energy flow. Related developments address LO energy-loss effects, anisotropic matter, collinear in-medium EECs, track functions in a hot QGP, EFT factorization, and energy-loss functions [143–147]. These

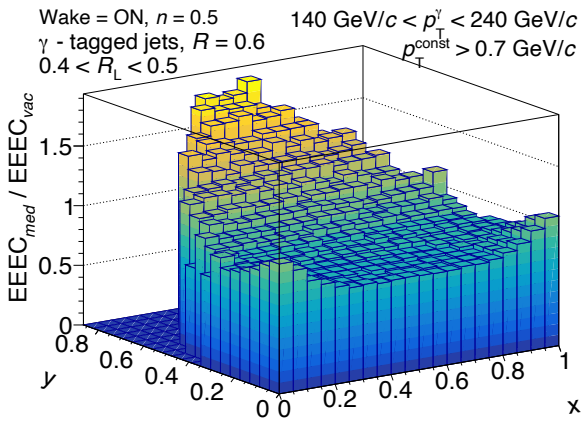

Fig. 8: Ratio of the shape-dependent three-point correlator in QGP and vacuum in the hybrid model. The enhancement is largest in regions where the wake contribution dominates over the modified parton shower. Figure reproduced from Ref. [138].

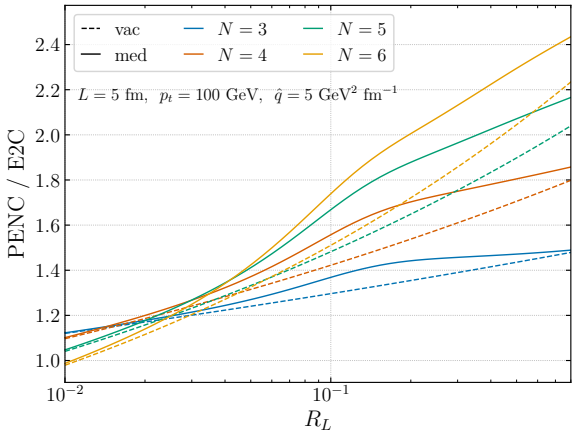

Fig. 9: Projected N-point energy correlators in vacuum and in medium. The medium modifies the scaling and angular structure of the correlator through both perturbative jet modification and hydrodynamic back-reaction. Figure reproduced from Ref. [141].

works address different components of the medium problem including wake-sensitive correlators, hydrodynamic back-reaction, in-medium collinear, evolution, charged-energy fractions, and energy-loss functions.

Cold nuclear matter supplies the baseline for the hot-medium program. In p-A and e-A collisions there is no long-lived QGP, but nuclear PDFs, multiple scattering, final-state interactions, and nuclear-size-enhanced higher-twist matrix elements can still modify the angular energy flow. These systems have the advantage that they can be organized within standard hard-scattering factorization [148, 149]. The higher-twist nuclear matrix elements needed for this description were developed long before modern EEC applications [150–162]. Energy correlators provide an angular observable in which such nuclear matrix elements can be organized and constrained. In e-A collisions, Devereaux, Fan, Ke, Lee, and Moult showed that the nuclear size is imprinted as an onset angle in the final-state energy flux, with an $A^{1/6}$ rescaling aligning the onset of medium modification for different nuclei in their eHIJING study [163]. Fu, Müller, and Sirimanna computed the jet EEC in cold nuclear matter at leading order in the jet-medium interaction and found that the modification depends on the jet energy, the scattering power of the cold medium, and the path length in the nucleus [164]. Barata, Kang, Mayo López, and Penttala extended the collinear EEC framework to single-inclusive jet production in p-p and p-A collisions, combining perturbative evolution with a nonperturbative model that covers the full angular region relevant for current measurements [27].

A complementary operator organization is available in the small-angle region. In this limit, the product of two energy-flow operators admits a light-ray OPE along the detector direction,

$$\lim_{n_1 \to n_2} \mathcal{E}(n_1)\mathcal{E}(n_2) = \frac{1}{\theta^2}\, \mathbb{O}^{[J=3]}_{\tau=2}(n_2) + \mathbb{O}^{[J=3]}_{\tau=4}(n_2) + \cdots , \tag{29}$$

where θ is the opening angle between the two detectors and $\mathbb{O}^{[J]}_{\tau}$ denotes a spin-J, twist-τ light-ray operator. This expansion is not a complete description of the nuclear modifications discussed above. Transport broadening, elastic scattering, wake dynamics, hydrodynamic response, flavor selection, track-function effects, and energy-loss bias enter through additional medium dynamics and through the state in

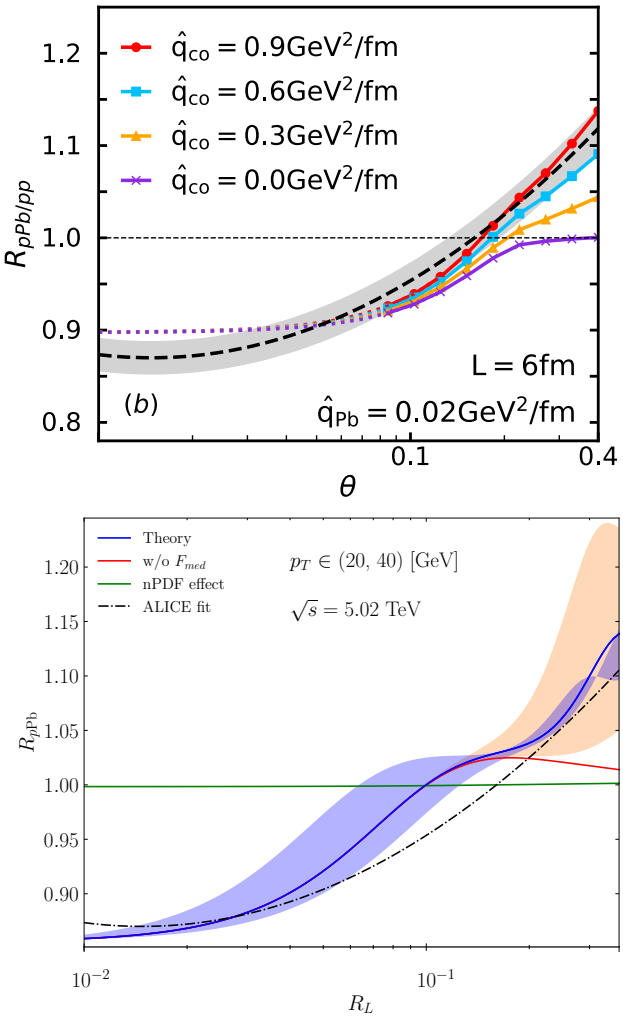

Fig. 10: Ratios of EECs in p-Pb and p-p collisions compared with theoretical descriptions of cold-nuclear-matter effects. Figures from Refs. [27, 164].

which the light-ray operators are evaluated. The OPE fixes the leading small-angle power structure and organizes the corresponding nuclear dependence into light-ray matrix elements. For a nuclear state compared with a p-p state, the same expansion gives, schematically,

$$\frac{\Sigma_{\text{nuc}}(\theta)}{\Sigma_{pp}(\theta)} \simeq \frac{A_2^{\text{nuc}}}{A_2^{pp}} \left[1 + \theta^2 \left(\frac{A_4^{\text{nuc}}}{A_2^{\text{nuc}}} - \frac{A_4^{pp}}{A_2^{pp}} \right) + \cdots \right], \tag{30}$$

where A_2^i and A_4^i denote the twist-two and twist-four light-ray matrix elements in the state $i = \text{nuc}, pp$, including the perturbative matching coefficients appropriate to the chosen normalization. After the leading normalization factor is removed, the first nuclear correction is therefore controlled by the difference of twist-four to twist-two matrix-element ratios and takes the form

$$\left[\frac{\Sigma_{\text{nuc}}(\theta)}{\Sigma_{pp}(\theta)} \right]_{\text{norm.}} \simeq 1 + a\,\theta^2 + \cdots . \tag{31}$$

Ref. [165] showed that this leading nuclear correction to the two-point EEC is consistent with an enhanced twist-four light-ray matrix element, producing a ratio of the form $1 + a\theta^2$, up to quantum corrections, and describing recent A-A and p-A data over the angular range used in current nuclear measurements. The OPE-based description isolates the leading small-angle power structure, while transport, hydrodynamic response, in-medium splitting, track functions, and energy-loss functions describe additional medium dynamics over the measured angular range.

Recent work has expanded these complementary descriptions. In the thin-medium regime, Ke, Mecaj, and Vitev [166] derived RG evolution for in-medium EEC jet functions in SCET [167–171] with Glauber exchange (SCET_G) [172, 173], computing one-loop jet functions with medium-induced splitting kernels at first order in opacity and identifying an angular and energy regime sensitive to medium-

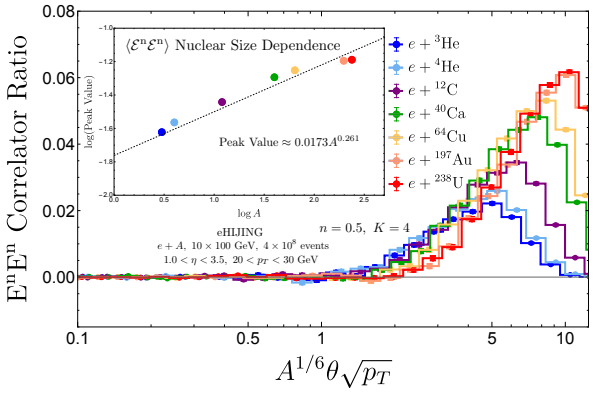

Fig. 11: Energy correlators in e-A collisions. Nuclear size is imprinted as an angular scale in the final-state energy flux, allowing different nuclear targets to leave distinguishable signatures. Figure reproduced from Ref. [163].

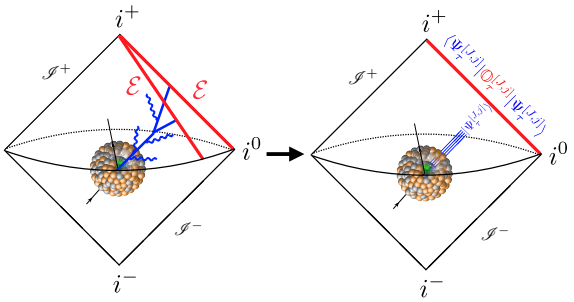

Fig. 12: Schematic light-ray-OPE organization of the small-angle two-point energy correlator in a nuclear state. The medium dependence enters through the expectation values of the light-ray operators. Figure reproduced from Ref. [165].

induced anomalous dimensions. Multiplicity-conditioned EEC jet functions give a separate perturbative handle on event selection: selecting jets at fixed normalized multiplicity changes the EEC anomalous dimension, which is relevant for controlling multiplicity-dependent biases in nuclear-environment measurements [174]. At small x, TEEC observables in electron-hadron, vector-boson-tagged hadron, and photon-hadron production probe dipole amplitudes and saturation dynamics [175–177]. One-point energy correlators (OPECs) in e-A collisions provide an inclusive probe of cold-nuclear-matter broadening and TMD-sensitive nuclear modification at EIC kinematics [43]. In the small-x CGC limit, the DIS OPEC probes saturation dynamics: the momentum-sum rule cancels the fragmentation-function dependence, leaving the dipole amplitude as the nonperturbative input [45]. Energy correlators therefore organize cold nuclear baselines, hot-medium response, wake dynamics, track effects, energy-loss bias, and higher-twist light-ray matrix elements in a common angular variable.

2.1.5 Energy correlators adapted for hadron structure

Recently, a growing body of work [29, 30, 32–37, 41, 42, 45, 52, 70] has extended the EEC paradigm to hadron-structure physics. In this setting, energy correlators serve both as more inclusive, calorimetric alternatives to observables built from identified hadrons or jets, and as genuinely new nonperturbative correlators of energy flow that complement conventional TMD PDFs and TMD FFs.

Nucleon energy correlators and target-fragmentation tomography

The nucleon energy correlator (NEC) was introduced as the DIS analogue of the EEC, with the energy-flow operator inserted between nucleon states rather than vacuum states [29]. This turns the standard EEC from final state correlations into an initial-final state correlator. In the Breit frame, with the incoming nucleon moving along the reference beam direction, the basic measurement is the solid angle distribution of the hadronic energy deposited in the target fragmentation region (TFR). A convenient energy-weight definition analogue to the standard EEC in Eq. (3) is

$$\frac{d\Sigma}{dQ^2\,dx_B\,d\Omega} = \sum_{i\in X}\int d\sigma(x_B, Q^2, p_i)\,\frac{E_i}{E_P}\,\delta(\Omega-\Omega_i)\,, \tag{32}$$

where $x_B = Q^2/(2P\cdot q)$ is the Bjorken variable, $Q^2 = -q^2$ is the virtuality of the virtual photon, E_P is the energy of the incoming nucleon, E_i is the energy of a detected final-state hadron, and Ω_i is the angle measured from the nucleon beam direction. For notational simplicity,

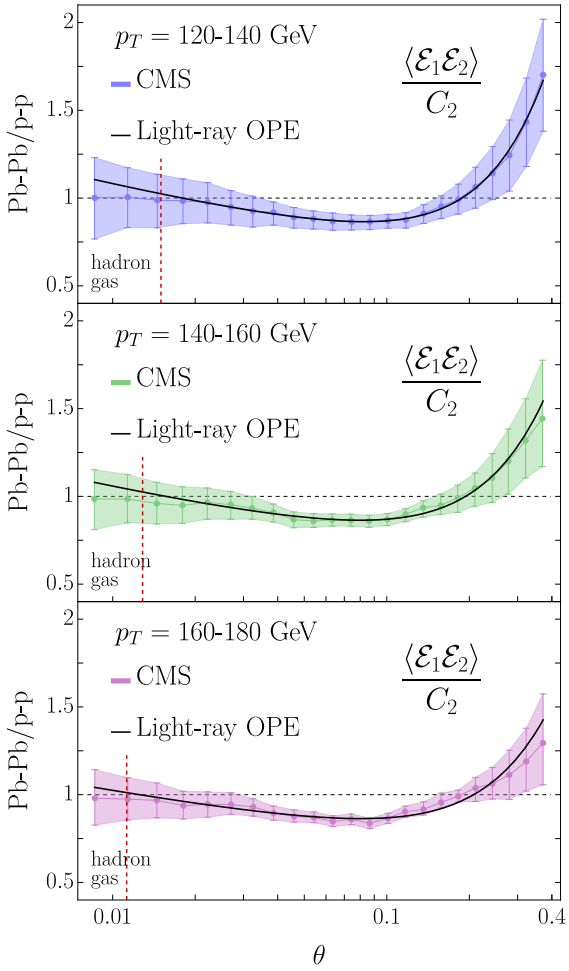

Fig. 13: Comparison of the nuclear-to-p-p EEC ratio with the light-ray-OPE scaling form. The OPE fixes the leading angular power of the short-distance correction, while the corresponding matrix element is determined from data. Figure reproduced from Ref. [165].

the dependence on the azimuthal angle is suppressed unless it is explicitly needed. The corresponding energy-flow operator acts as

$$\frac{1}{E_P}\mathcal{E}(\hat{\Omega})\,|X\rangle = \sum_{i\in X}\frac{E_i}{E_P}\,\delta(\Omega-\Omega_i)\,|X\rangle. \tag{33}$$

The DIS energy pattern can therefore be written as the hadronic tensor with an inserted energy-flow operator,

$$\frac{d\Sigma}{dQ^2\,dx_B\,d\Omega} = \frac{\alpha_{\rm em}^2}{Q^4}L_{\mu\nu}\int d^4y\,e^{iq\cdot y}\,\frac{1}{E_P}\langle P|j^{\mu\dagger}(y)\,\mathcal{E}(\hat{\Omega})\,j^{\nu}(0)|P\rangle, \tag{34}$$

where $L_{\mu\nu}$ is the lepton tensor and j^μ is the electromagnetic current. Equation (34) makes the main distinction from a standard final-state EEC explicit. The energy measurement is still calorimetric and inclusive, but the matrix element now probes how a struck parton is correlated with the angular energy distribution of the target remnant.

The distinction is the most manifest in the TFR, where the hard scattering and target fragmentation are separated by the Bjorken limit. The leading-power factorization has the form [29, 31]

$$\frac{d\Sigma}{dQ^2\,dx_B\,d\Omega} = \sum_a\int_{x_B}^1\frac{d\xi}{\xi}\,\hat{\sigma}_a\!\left(\frac{x_B}{\xi},Q,\mu\right)f_a^{\mathcal{E}}(\xi,\Omega,\mu)+\mathcal{O}\!\left(\frac{\Lambda_{\rm QCD}}{Q}\right), \tag{35}$$

where $a=q,\bar{q},g$ labels the struck parton, H_a is the same short-distance partonic cross section that appears in inclusive DIS and the new non-perturbative object, the unpolarized nucleon energy correlator (NEC) is introduced as

$$f_q^{\mathcal{E}}(x,\Omega) = \int\frac{dy^-}{4\pi}\,e^{-ixP^+y^-}\langle P|\bar{\psi}(y^-)\,W^\dagger(y^-)\frac{\gamma^+}{2}\,\frac{\mathcal{E}(\Omega)}{P^+/2}\,W(0)\psi(0)|P\rangle\,, \tag{36}$$

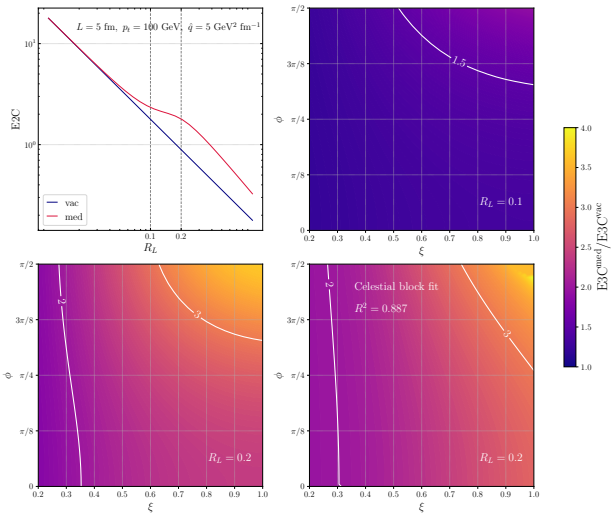

Fig. 14: Medium modification of three-point energy correlators. The two-point correlator identifies the angular scale of nuclear modification; the three-point correlator probes the radiation pattern and wake contribution at that scale. Figure reproduced from Ref. [141].

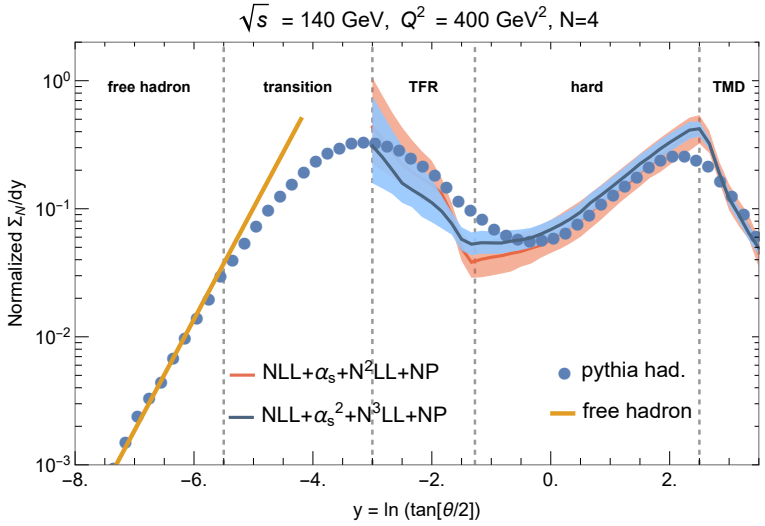

Fig. 15: The unpolarized NEC spectrum, first predicted in Ref. [32]. The spectrum prediction for longitudinal polarized NEC with NNLL in the TFR and N^{3}LL in the CFR can be found in [33]. Figure courtesy of H. Cao.

for the quark NEC and the gluon NEC can be found in Ref. [31]. Here W stands for the collinear Wilson line. Its extension to other spin effects such as the Sivers effect, the proton longitudinal spin are also discussed in the literature [29, 33, 178, 179]

The factorization theorem and the operator definition indicate that the nucleon energy correlator in the TFR is controlled by collinear dynamics, in close analogy with the small-angle EEC. In this case, the transverse structure of the target is not accessed through an explicit transverse-momentum measurement, but through the angular distribution of the measured energy flow.

Figure 15 [32] shows the NEC distribution over the full polar-angle range at EIC kinematics, obtained from Pythia simulations and perturbative-QCD calculations. The NEC spectrum displays the same qualitative pattern as the EEC distribution. In the TFR, the small-angle limit $\theta \to 0$ is characterized by the perturbative scaling $d\Sigma/d\theta \sim \theta^{-1+\gamma}$, where the anomalous dimension γ is generated by DGLAP-like evolution and is determined by the spacelike splitting functions. Deviations from this scaling mark the transition from partonic to hadronic degrees of freedom. At still smaller angles, where the post-confinement domain is reached, the NEC develops an approximately uniform distribution, paralleling the plateau observed in the small-angle EEC.

Compared with the standard EEC, however, the nonperturbative structure of the NEC remains largely unexplored. A systematic study of the NEC would therefore provide a complementary probe of nucleon structure. One concrete example is its recently established connection to fracture functions [178, 180]. This connection, in turn, offers a natural framework for analyzing the post-confinement scaling of the NEC, in close analogy with the role of DiFFs in the small-angle EEC.

Moreover, because the NEC is collinear, it is largely free from Sudakov suppression and robust against soft contamination, making it an useful probe of the nucleon's intrinsic spin structure. As an illustration, Ref. [101] showed that, in DIS, measuring the energy-energy correlator with one detector b in the central region and the other detector a in the TFR probes linear gluon polarization through the $\cos(2\phi)$ modulation implied by the factorization theorem

$$\frac{d\Sigma}{dx_B dQ^2 d\theta_a d\theta_b d\phi}\Big|_{\theta_b\gg\theta_a\to 0} = \frac{4\pi\alpha_{\rm em}^2 e_q^2}{Q^4}\int\frac{dz}{z}\hat{H}_i(z,y,\theta_b)\frac{x_B}{z}f_i^{\mathcal{E}}\left(\frac{x_B}{z},\theta_a^2\right)+\frac{1}{2}\cos(2\phi)\Delta\hat{H}(z,y,\theta_b)\frac{x_B}{z}d_g^{\mathcal{E}}\left(\frac{x_B}{z},\theta_a^2\right) \tag{37}$$

where $\phi=\phi_a-\phi_b$, and $d_g^{\mathcal{E}}$ denotes the linearly polarized component of the gluon NEC [101]

$$f_g^{ij,\mathcal{E}}(x,\Omega)=\frac{\delta_T^{ij}}{2}f_g^{\mathcal{E}}(x,\theta^2)+\left(n_T^i n_T^j-\frac{\delta_T^{ij}}{2}\right)d_g^{\mathcal{E}}(x,\theta^2)\,, \tag{38}$$

where n_T is the transverse unit vector pointing along the energy flow. Although Eq. (37) resembles the naive TMD expression for dijet probes of linearly polarized gluons, its angular structure is more rigid and holds to all orders. In the small-θ_a limit, factorization separates the sector associated with energy flow a from the hard tensor that fixes direction b. The a-dependence is contained in the linearly polarized gluon NEC, while the b-dependence enters through the hard scattering. The only leading-power contraction of the two traceless transverse tensors is $\left(\hat{n}_a^i\hat{n}_a^j-\frac{\delta_T^{ij}}{2}\right)\left(\hat{n}_b^i\hat{n}_b^j-\frac{\delta_T^{ij}}{2}\right)=\frac{1}{2}\cos(2\phi)$. Radiative corrections can change the scalar coefficient, but not the harmonic. This differs from ordinary TMD dijet observables, where soft radiation can correlate the two measured transverse directions and generate a less constrained angular dependence [181].

Other advantages of the NEC, including probing the onset of gluon saturation [30], the small-x odderon [34], and a pivotal avenue for delving into quantum entanglement and scrutinizing the Bell inequality at high-energy colliders [182] have also been explored recently in the literature. The connection of the NEC to the transverse momentum moments (TMMs) of the TMD distributions has also been established [35] and will be discussed later.

The NEC construction has also been used to probe chirality-flipping interactions in ep collisions [179]. The light-quark electroweak dipole operators may be written as

$$\mathcal{L}_{\rm dipole}=\frac{1}{\Lambda^2}\left[C_{uB}\,\bar{Q}\sigma^{\mu\nu}u_R\,\widetilde{H}\,B_{\mu\nu}+C_{uW}\,\bar{Q}\sigma^{\mu\nu}\tau^I u_R\,\widetilde{H}\,W^I_{\mu\nu}+C_{dB}\,\bar{Q}\sigma^{\mu\nu}d_R\,H\,B_{\mu\nu}+C_{dW}\,\bar{Q}\sigma^{\mu\nu}\tau^I d_R\,H\,W^I_{\mu\nu}\right]+\text{h.c.}\,. \tag{39}$$

In ordinary unpolarized inclusive DIS, the interference of these chiral-odd amplitudes with the Standard Model is suppressed. A chiral-odd NEC avoids this suppression by using the azimuthal direction of the target-side energy flow as a transverse-spin analyzer, restoring the leading interference term for new-physics dipole operators without requiring a polarized nucleon beam or identified final-state hadrons. The relevant quark transversity NEC has the form

$$\epsilon_\perp^{ij}n_{T,j}\,h_{1,q}^{\perp\mathcal{E}}(x,\theta)=\int\frac{dy^-}{4\pi}e^{-ixP^+y^-}\langle P|\bar{\psi}(y^-)\,W^\dagger(y^-)[i\sigma^{j+}\gamma_5]\,\frac{\mathcal{E}(\Omega)}{P^+/2}\,W(0)\psi(0)|P\rangle\,, \tag{40}$$

so that the dipole-SM interference generates $\cos\phi$ and $\sin\phi$ calorimetric asymmetries,

$$A_{\mathcal{E}}^{\sin\phi},A_{\mathcal{E}}^{\cos\phi}\sim\frac{h_{1,q}^{\perp\mathcal{E}}(x,\theta)}{f_q^{\mathcal{E}}(x,\theta)}\,\frac{Q\,v}{\Lambda^2}\,\text{Re/Im}\,C_{q\gamma,qZ}. \tag{41}$$

Here v is the Higgs vacuum expectation value and $C_{q\gamma,qZ}$ denote the photon and Z-dipole combinations after electroweak symmetry breaking. The size of the dipole-SM interference can be estimated using the relation between the NEC and the Boer-Mulders TMD transverse-momentum moment (TMM) [35], with existing TMD extractions as nonperturbative input [183–185]. The resulting calorimetric azimuthal asymmetries require neither a polarized proton beam nor identified final-state hadrons. This makes the observable experimentally simpler than single transverse spin asymmetry and dihadron-based proposals and applicable not only at the EIC but also to the existing HERA data. The projected EIC reach is competitive with, and in several comparisons stronger than, existing LHC Drell-Yan bounds [186], see Fig. 16, and proposed EIC dihadron probes [187], while retaining separate sensitivity to the real and imaginary parts of the light-quark dipole couplings.

Semi-inclusive energy correlators and TMD transverse-momentum moments

Semi-inclusive energy correlators (SIECs) extend the NEC by correlating a reference hadron with the surrounding energy flow [35]. The basic idea is to correlate a reference hadron with the energy flow carried by the radiation surrounding it. If the reference hadron is the incoming proton, the observable reduces to the NEC in the target fragmentation region. If the reference hadron is an identified final-state hadron, the same construction defines the fragmenting energy correlator [35, 36] in the current or jet fragmentation region. The two cases could be written in parallel as

$$\frac{d\Sigma_{\rm TFR}}{d\sigma}=\int d\Omega\,w(\Omega)\,\frac{1}{E_P}\mathcal{E}(\Omega)\qquad\text{and}\qquad\frac{d\Sigma^h_{\rm CFR}}{d\sigma^h}=\int d\Omega_h\,w(\Omega_h)\,\frac{1}{E_h}\mathcal{E}(\Omega_h), \tag{42}$$

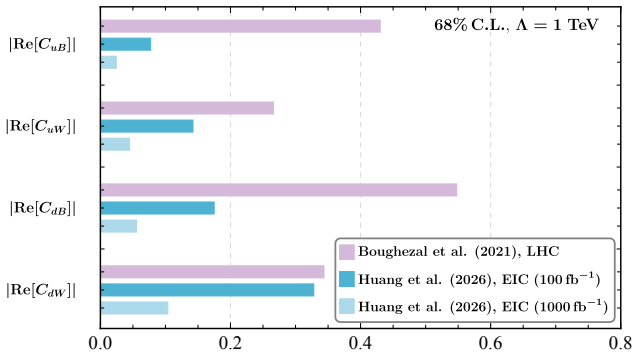

Fig. 16: Comparison between the NEC single-operator constraints at the EIC and those reported in Ref. [186] based on Drell-Yan measurements at the LHC. Figure courtesy of Y. Huang, X. Tong and H. Wang [179].

where w is an angular weight, Ω is measured with respect to the incoming proton in the first case, and Ω_h is measured with respect to the identified hadron in the second case. In the small-angle limit, their factorization takes the form

$$d\Sigma_{\rm TFR} = \sum_a \hat{\sigma}_a \otimes f_a^{\mathcal{E}} + O\left(\frac{\Lambda_{\rm QCD}}{Q}\right), \qquad d\Sigma^h_{\rm CFR} = \sum_a d\hat{\sigma}_a \otimes D^{\mathcal{E}}_{h/a} + O\left(\frac{\Lambda_{\rm QCD}}{Q}\right). \tag{43}$$

where the corresponding nonperturbative objects are the NEC $f_a^{\mathcal{E}}$ and the fragmenting energy correlator $D^{\mathcal{E}}_{h/a}$ whose operator definition can be found in [35, 36]. A related example is the quarkonium energy correlator [188], which measures the energy flow at an angular distance from an identified quarkonium and provides a probe of the energy pattern associated with heavy-quark hadronization.

A key observation of Ref. [35] is that, in the massless limit, the transverse momentum of a state $|X\rangle$ can be expressed in terms of the energy-flow operator as

$$\vec{k}_T = \int d\Omega \, \langle X|\mathcal{E}(\Omega)\, \vec{n}_T|X\rangle\,, \qquad \vec{n}_T = (\cos\phi, \sin\phi)\,, \tag{44}$$

Therefore, the relation of SIECs to TMMs immediately follows, such that

$$\int d^2\vec{k}_T \, k_T^{i_1} \cdots k_T^{i_N} \, F_{a/P}(x, \vec{k}_T) = (P^+)^N \int \prod_{\ell=1}^{N} d\Omega_\ell \, n_\ell^{i_\ell, T} \, f_a^{\mathcal{E}\cdots\mathcal{E}}(x, \Omega_1, \ldots, \Omega_N) + \text{p.c.}\,, \tag{45}$$

where $F_{a/P}$ denotes a generic TMD PDF, $f_a^{\mathcal{E}\cdots\mathcal{E}}$ is the N-point NEC, and "p.c." denotes perturbatively calculable corrections associated with restricting the angular measurement to the collinear region. The connection was used to estimate the size of the BSM dipole-SM interference in Ref. [179]. Similar relation holds for the TMD FFs and fragmenting energy correlators [35].

More generally, by varying the angular weight $w(\Omega)$, one selects different structures of the radiation pattern. As an example, for a transversely polarized target one may choose the azimuthal weight $w^{f_1^\perp}(\Omega) = \frac{d\Omega}{\pi}\, \epsilon_t^{\mu\nu} n_{t,\mu} s_{t,\nu}$, with the transverse spin vector s_t and $\epsilon_t^{\mu\nu}$ the antisymmetric tensor in the transverse plane, to measure the Sivers effects through the target-side NEC

$$\int w^{f_1^\perp}(\Omega)\, f_q^{\mathcal{E}}(x, \Omega) \;=\; \int \frac{dk_t^2}{2M}\, k_t^2 f_{1T}^\perp(x, k_t). \tag{46}$$

Fragmentation-side weights isolate Collins-sensitive moments in the same spirit [35, 37].

One point energy correlator

The one-point energy correlator (OPEC) is the simplest member of the energy-correlator family. Instead of measuring pairwise energy correlations, it measures the angular distribution of energy flow relative to a chosen reference direction. For the OPEC induced by a vector current like in e^+e^- annihilation, rotational invariance and energy positivity fix the one-point energy distribution up to a single parameter [6, 39, 189, 190]

$$\langle \mathcal{E}(\hat{n})\rangle = \frac{\langle E\rangle}{4\pi}\left[1 + a_{\mathcal{E}}\left(\frac{3}{2}\sin^2\theta - 1\right)\right], \qquad -\frac{1}{2} \le a_{\mathcal{E}} \le 1\,, \tag{47}$$

where θ is measured from the beam axis. The two endpoints are saturated by free theories with different matter content. QCD therefore gives a particularly interesting realization of this observable. At short distances the vector current creates quark degrees of freedom, while at long distances confinement converts the same energy distribution into hadronic states. The parameter $a_{\mathcal{E}}$ then interpolates between the fermionic and scalar-like extremal correlators. This flow can be reconstructed by matching perturbative QCD at short distances to chiral perturbation theory in the hadronic regime, making the OPEC a direct probe of how confinement reshapes the angular structure of energy flow.

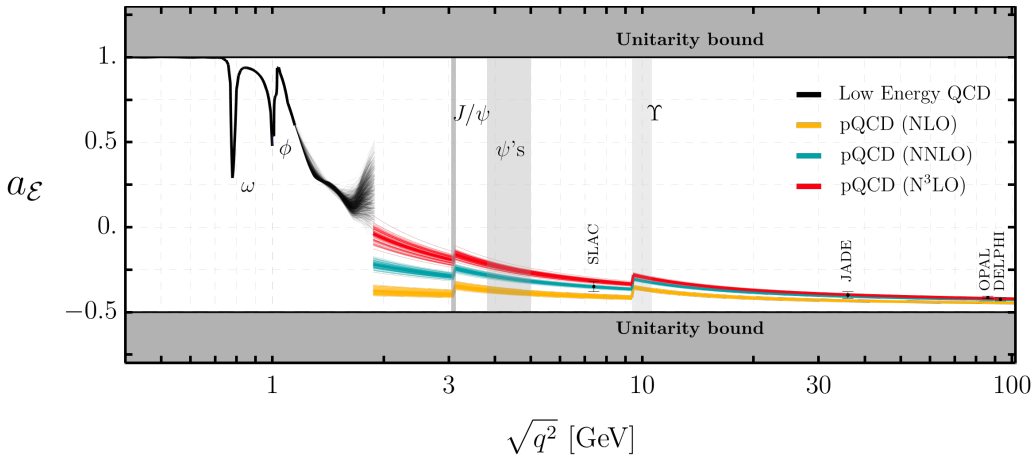

Fig. 17: QCD flow of the OPEC parameter $a_{\mathcal{E}}$ as a function of the center-of-mass energy. The gray regions are excluded by the energy-positivity bound $-1/2 \le a_{\mathcal{E}} \le 1$. The black band denotes the low-energy QCD reconstruction, while the colored curves show perturbative-QCD predictions at increasing fixed-order accuracy. Existing indirect determinations from SLAC, JADE, OPAL, and DELPHI are also shown. The low-energy and charmonium regions are especially important for testing how the fermionic short-distance energy flow is reorganized into hadronic degrees of freedom. Figure from Ref. [39].

Fig. 17 shows the QCD flow of $a_{\mathcal{E}}$. At large timelike momentum transfer, the electromagnetic current resolves quark degrees of freedom and $a_{\mathcal{E}}$ approaches the fermionic side of the allowed region. At low energies, the same current produces a small number of exclusive hadronic channels, with several channels fixed by symmetry near the extremal boundaries. Two-pseudoscalar states saturate the upper endpoint, while three-pseudoscalar and vector-pseudoscalar channels are driven toward the lower endpoint by the anomalous Wess-Zumino-Witten structure [39]. The motion of $a_{\mathcal{E}}$ therefore gives a one-parameter measure of how confinement reorganizes angular energy flow.

Existing information on $a_{\mathcal{E}}$ is indirect, relying on recast longitudinal-fragmentation measurements or related inclusive observables. A direct OPEC measurement would instead determine the angular energy flow itself and test the confinement-driven flow shown in Fig. 17. BESIII, and in the future the Super Tau-Charm Facility, cover the timelike region where $a_{\mathcal{E}}$ should be most sensitive to the change from exclusive hadronic production to quark-level continuum dynamics [191, 192].

The OPEC can also be measured within a jet, with the angle measured from the jet axis. For the conventional anti-k_T jet, the OPEC follows the standard TMD factorization and offers a new venue to the TMD distributions [38, 40, 41]. A particularly clean spin application was proposed in transversely polarized $p^\uparrow p$ collisions [41]. The azimuthal dependence of the OPEC distribution has the form

$$\frac{d\Sigma_{\rm OPEC}}{d\theta_n d\phi_n d\eta dp_T} = Z_{UU} + Z_{UT}\ \sin(\phi_s - \phi_n)\,, \tag{48}$$

where ϕ_s is the azimuthal angle of the proton spin and ϕ_n is the azimuthal angle of the measured energy flow. The spin-dependent Z_{UT} structure functions take the factorized form contains the transversity distribution $h_1^q(x)$ convoluted with a perturbative spin-transfer coefficient and an OPEC jet function,

$$Z_{UT} = \theta_n \frac{\alpha_s^2}{s} p_T^2 \sum_{a,b,c} h_1^a(x,\mu) \otimes f_b(x,\mu) \otimes \Delta\hat{H}^{\rm Collins}_{ab\to c}(\mu) \otimes p_T\theta_n \mathcal{J}_c^{\mathcal{E}}(\theta_n,\mu) + O\left(\frac{\Lambda_{\rm QCD}}{p_T\theta_n}\right), \tag{49}$$

where $\Delta\hat{H}^{\rm Collins}$ represents the spin-dependent partonic matrix elements and $\mathcal{J}_c^{\mathcal{E}}$ is the OPEC fragmenting jet function can be shown related to the TMD Collins function. It therefore probes transversity $h_1^a(x,\mu)$ through the angular flow of jet energy rather than through the transverse momentum of a single identified hadron. Compared with identified-hadron Collins asymmetries, the energy-flow measurement is IRC safe and can access much smaller angular scales. The similar one-point structure has also been used to study gluon polarization in the initial target [42], which provides a gluon polarimetry with OPEC without relying on complex declustering or tagging algorithms. Inspired by Ref. [41], STAR measured OPEC spin asymmetries in transversely polarized pp collisions at $\sqrt{s} = 200$ GeV using π^+ and π^- energy flow [44]; see Fig. 18. Similar and larger asymmetries were also observed in EEC measurements based on $\pi^+\pi^-$ pairs [41].

2.2 Novel methods beyond Energy Correlators

Jet substructure provides a more traditional route to the same energy-flow information inside jets. Its observables probe QCD radiation through jet shapes, grooming, splitting variables, charges, and flavor tags [1, 2, 193–199]. Track-based measurements can be described with track-function factorization [200], while recoil-free axes define a class of angular observables in which soft recoil is reduced by construction [201]. In hadron-structure and nuclear applications, different jet-substructure measurements separate different combinations of recoil, flavor, mass, and medium response.

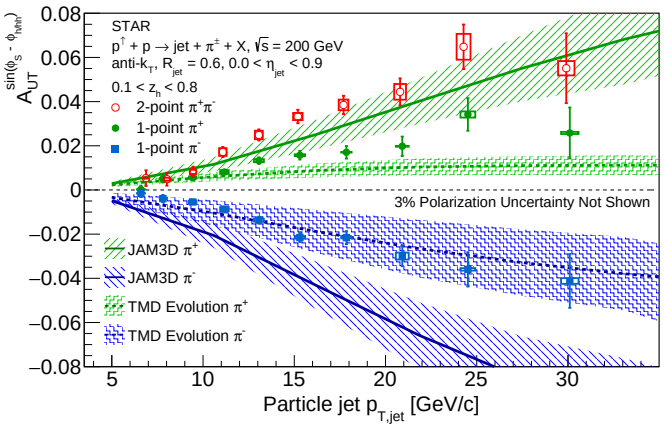

Fig. 18: Spin asymmetries measured by STAR using OPEC and EEC on π^+, π^- in $p^\uparrow p$ collisions. Figure reproduced from [41].

A representative example is Soft Drop [199], which isolates the first sufficiently hard splitting in the reclustered jet. One defines

$$z_g = \frac{\min(p_{T1}, p_{T2})}{p_{T1} + p_{T2}}, \qquad R_g = \Delta R_{12}, \qquad z_g > z_{\rm cut}\left(\frac{R_g}{R}\right)^\beta, \tag{50}$$

where $p_{T1,2}$ are the transverse momenta of the two branches that first satisfy the grooming condition, R_g is their opening angle, R is the original jet radius, and $(z_{\rm cut}, \beta)$ specify the grooming cut. The same radiation pattern may be projected onto jet angularities, energy-correlation functions, and jet charge,

$$\lambda_\alpha = \sum_{i\in J} z_i \theta_i^\alpha, \qquad e_2^{(\alpha)} = \sum_{i<j\in J} z_i z_j \theta_{ij}^\alpha, \qquad Q_\kappa = \sum_{i\in J} q_i z_i^\kappa, \tag{51}$$

with $z_i = p_{Ti}/p_{TJ}$, q_i the electric charge of constituent i, and θ_i or θ_{ij} denoting angles measured relative to a chosen jet axis or between jet constituents. These observables are complementary: λ_α probes the radial energy profile, $e_2^{(\alpha)}$ emphasizes correlated prongs, and Q_κ tags flavor flow. Energy correlators belong to this broader class of weighted radiation observables, distinguished by their direct formulation in terms of energy flow and by their simple infrared-safe weighting.

For hadron structure, the most direct use of substructure is hadron-in-jet production [202]. In this case the jet fixes the hard collinear direction, while the identified hadron probes fragmentation at fixed longitudinal fraction and transverse momentum relative to the jet axis. Schematically,

$$d\sigma(pp \to (\text{jet}\, h)X) \sim \sum_{abc} f_a \otimes f_b \otimes H_{ab\to c} \otimes \mathcal{G}_{c\to h}(z, j_T, R, \mu), \tag{52}$$

where $\mathcal{G}_{c\to h}$ denotes a fragmenting-jet function or, for the transverse momentum j_T measured from the standard jet axis, when $j_T \ll p_T R$, a TMD fragmenting-jet function matched onto ordinary TMD fragmentation functions. The formalism developed from the original hadron-in-jet construction to fragmenting-jet functions and then to TMD fragmenting-jet functions [202–208]. It now provides a common framework for longitudinal fragmentation fits, Collins and polarizing asymmetries, and transverse-momentum measurements inside jets [205–214]. Experimentally, STAR has already measured azimuthal asymmetries of hadrons inside jets, while future EIC measurements can extend these tests to a cleaner lepton-hadron environment [215–219]. A complementary flavor-sensitive direction is jet charge. After its classic introduction and modern factorized formulation [220–222], jet charge was proposed as a flavor prism for TMD and spin studies at the EIC [223]. Recent work on medium-modified and nonperturbative jet charge has sharpened both the phenomenological optimization and the theoretical interpretation of this observable [224, 225].

At the EIC and in cold nuclear matter, jet substructure helps separate initial-state nuclear PDFs from final-state broadening and hadronization. Jet angularities in photoproduction already show sensitivity to the EIC environment [226]. An interesting related example is the use of 0-jettiness as an event-shape veto to isolate intrinsic TMD dynamics. The calculation uses a joint-resummation framework for the logarithms associated with both the veto scale and the vector-boson transverse momentum, and the same veto logic was also discussed as a tool for spin-dependent measurements at the EIC [227]. Ref. [227] showed that imposing a 0-jettiness cut suppresses initial-state radiation in TMD observables and can substantially enhance transverse single-spin asymmetries in $W^\pm$ and Z^0 production at RHIC. In particular, the $W^\pm$ SSA at $q_\perp = 5$ GeV and central rapidity $y = 0$ was found to increase by about 115%, strengthening the sensitivity to the predicted Sivers-function sign change. The dependence for $W^\pm$ SSA on the 0-jettiness cut with $q_\perp$ integrated over 1 GeV $< q_\perp <$ 6 GeV is illustrated in Fig. 19. As the veto is tightened, the oscillation amplitude of A_N increases, while the inclusive limit shows a more diluted spin asymmetry. This pattern suggests a possible physical reading of event-shape cuts as a dial on the radiation environment seen by the measured TMD observable. A tighter veto reduces the phase space for unresolved radiation that can recoil against, and thereby dilute, the spin-dependent transverse-momentum correlation. In this restricted sense, the role of 0-jettiness is analogous to the controlled decoher-

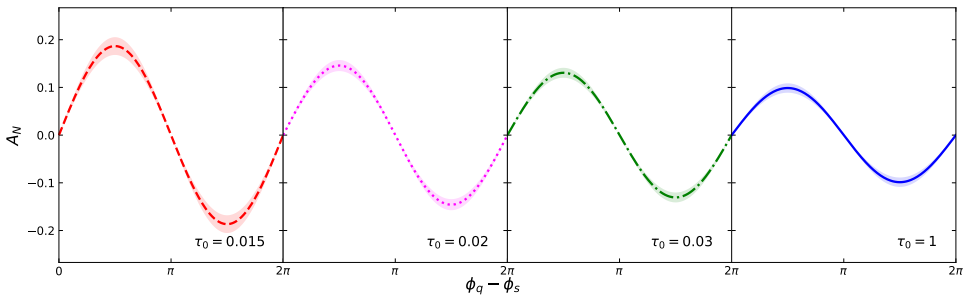

Fig. 19: Transverse single-spin asymmetry A_N as a function of the azimuthal angle difference $\phi_q - \phi_S$ for different 0-jettiness cuts τ_0 [227]. The tighter vetoes, such as $\tau_0 = 0.015$, give a larger modulation than the more inclusive case $\tau_0 = 1$, showing how the measured spin asymmetry depends on the amount of allowed radiation. Figure courtesy of D. Y. Shao.

ence of matter-wave interference by environmental radiation [228], where changing the coupling to emitted radiation changes the observed interference contrast [229]. Whether this interpretation can be made more quantitative, and how it can be tested experimentally, remain interesting questions for future study.

Along the cold-nuclear-matter jet direction, Refs. [230, 231] studied inclusive jet and jet-charge production in $e + A$, and then heavy-flavor jet rates and groomed substructure, thereby establishing a systematic SCET-with-Glauber framework for cold-matter jet tomography. Machine-learning-based jet and event classifiers have also been proposed at the EIC to enhance flavor separation and process identification in hadron-structure and spin measurements [232].

Heavy-flavor tagging adds a second perturbative lever arm through the quark mass and makes the dead-cone region directly accessible. The theoretical and experimental program has progressed from semi-inclusive heavy-flavor jet functions in pp and heavy-ion collisions to prompt b-jet substructure, Soft-Drop analyses of heavy-flavor jets, and fully differential heavy-flavour jet-substructure calculations [233–237]. This direction is directly relevant for both eA and AA studies, since mass effects help disentangle broadening, energy loss, and fragmentation from genuinely medium-induced modifications.

In heavy-ion collisions, grooming and resolved-branching observables turn jet quenching from an inclusive suppression problem into a differential probe of coherence, formation time, and medium response. Measurements of z_g, R_g, groomed mass, subjet fragmentation, jet shapes, and angularities are now available in Pb-Pb and Au-Au systems [238–243]. The theoretical picture combines vacuum-like and medium-induced emissions, color decoherence, recoil and wake effects, and dynamically groomed scales [105, 244–253]. The observable dependence is essential: z_g is closely connected to the splitting function, R_g to the medium resolution angle, groomed mass and $k_{T,g}$ to hard transverse kicks, and heavy-flavor-tagged substructure to the interplay of dead-cone physics and in-medium branching. Recent work has made the bridge back to correlator-based observables explicit, showing how jet shapes, substructure observables, and energy correlators probe complementary aspects of the in-medium radiation pattern [143].

3 Conclusions and outlook

Energy correlators expose the scale dependence of final-state QCD through angles. Their angular distributions trace intrinsic QCD scales, from perturbative radiation to post-confinement energy flow. Light-ray operators provide a natural description of the energy correlators, as in conformal-collider analyses of energy flow. The corresponding OPE relates angular scaling to anomalous dimensions in the perturbative region and to hadronic matrix elements in the long-distance region. Through the energy correlators, this operator framework provides a new tool for studying nonperturbative QCD in measured hadronic final states.

Energy-flow correlations also retain tensor and spin information. At small angles, the relevant structures are governed by collinear dynamics and are not mixed with leading soft recoil. They can probe spin-dependent angular structures in regimes where ordinary transverse-momentum measurements are affected by recoil. In the back-to-back region, recoil enters at leading power, and the EEC connects with TMD factorization through Collins-Soper evolution.

The same final-state radiation can be constrained with more exclusive jet observables. Axes, grooming, subjet kinematics, jet charge, flavor tags, and identified hadrons provide experimental control over the radiation pattern and the hadronization history of a jet. Energy correlators supply the inclusive angular moments and the operator interpretation. Used in this form, these measurements open new ways to study hadron structure, nuclear structure, nuclear matter, spin-dependent final-state dynamics, and jet formation in QCD.

Acknowledgments

We thank Haotian Cao, Yingsheng Huang, Ding Yu Shao, Xuan-Bo Tong, Hao-Lin Wang for sharing figure material used in this review and for helpful discussions. We acknowledge the use of ChatGPT (`GPT-5.5 Thinking`, OpenAI) for assistance with literature

research and discussions on manuscript organization. X. L. is supported by the National Natural Science Foundation of China under Grant No. 12547109 and Fundamental Research Funds for the Central Universities, Beijing Normal University. H. X. Z is supported by the National Natural Science Foundation of China under grant No. 12425505. I. M. is supported by the Sloan Foundation.

References

[1] Andrew J. Larkoski, Ian Moult, and Benjamin Nachman. Jet Substructure at the Large Hadron Collider: A Review of Recent Advances in Theory and Machine Learning. *Phys. Rept.*, 841:1–63, 2020.
[2] Roman Kogler et al. Jet Substructure at the Large Hadron Collider: Experimental Review. *Rev. Mod. Phys.*, 91(4):045003, 2019.
[3] Ian Moult and Hua Xing Zhu. Energy Correlators: A Journey From Theory to Experiment. 6 2025.
[4] C. Louis Basham, Lowell S. Brown, S. D. Ellis, and S. T. Love. Electron - Positron Annihilation Energy Pattern in Quantum Chromodynamics: Asymptotically Free Perturbation Theory. *Phys. Rev. D*, 17:2298, 1978.
[5] C. Louis Basham, Lowell S. Brown, Stephen D. Ellis, and Sherwin T. Love. Energy Correlations in electron - Positron Annihilation: Testing QCD. *Phys. Rev. Lett.*, 41:1585, 1978.
[6] Diego M. Hofman and Juan Maldacena. Conformal collider physics: Energy and charge correlations. *JHEP*, 05:012, 2008.
[7] Simon Caron-Huot, Murat Kologlu, Petr Kravchuk, David Meltzer, and David Simmons-Duffin. Detectors in weakly-coupled field theories. *JHEP*, 04:014, 2023.
[8] Lance J. Dixon, Ian Moult, and Hua Xing Zhu. Collinear limit of the energy-energy correlator. *Phys. Rev. D*, 100(1):014009, 2019.
[9] Hao Chen. QCD factorization from light-ray OPE. *JHEP*, 01:035, 2024.
[10] Patrick T. Komiske, Ian Moult, Jesse Thaler, and Hua Xing Zhu. Analyzing N-Point Energy Correlators inside Jets with CMS Open Data. *Phys. Rev. Lett.*, 130(5):051901, 2023.
[11] Shreyasi Acharya et al. Exposing the parton-hadron transition within jets with energy-energy correlators in pp collisions at $\sqrt{s} = 5.02$ TeV. 9 2024.
[12] B. E. Aboona et al. Measurement of Two-Point Energy Correlators within Jets in p+p Collisions at s=200 GeV. *Phys. Rev. Lett.*, 135(11):111901, 2025.
[13] Hannah Bossi et al. Energy Correlators from Partons to Hadrons: Unveiling the Dynamics of the Strong Interactions with Archival ALEPH Data. 10 2025.
[14] Xiaohui Liu, Werner Vogelsang, Feng Yuan, and Hua Xing Zhu. Universality in the Near-Side Energy-Energy Correlator. *Phys. Rev. Lett.*, 134(15):151901, 2025.
[15] Kyle Lee and Iain W. Stewart. Dihadron Fragmentation and the Confinement Transition in Energy Correlators. *Phys. Rev. Lett.*, 136(8):081902, 2026.
[16] Cyuan-Han Chang, Hao Chen, Xiaohui Liu, David Simmons-Duffin, Feng Yuan, and Hua Xing Zhu. Quantum Scaling in Energy Correlators beyond the Confinement Transition. *Phys. Rev. Lett.*, 136(8):081903, 2026.
[17] Yuxun Guo, Feng Yuan, and Wenbin Zhao. Factorization and Resummation for the Nearside Energy-Energy Correlators. *Phys. Rev. Lett.*, 136(8):081904, 2026.
[18] Zhong-Bo Kang, Andreas Metz, Daniel Pitonyak, and Congyue Zhang. Dihadron Fragmentation Framework for Near-Side Energy-Energy Correlators. *Phys. Rev. Lett.*, 136(8):081905, 2026.
[19] Enrico Herrmann, Zhong-Bo Kang, Jani Penttala, and Congyue Zhang. Collinear limit of the energy-energy correlator in e^+e^- collisions: transition from perturbative to non-perturbative regimes. 7 2025.
[20] Max Jaarsma, Yibei Li, Ian Moult, Wouter J. Waalewijn, and Hua Xing Zhu. From DGLAP to Sudakov: Precision Predictions for Energy-Energy Correlators. 12 2025.
[21] John C. Collins and Davison E. Soper. Back-To-Back Jets in QCD. *Nucl. Phys. B*, 193:381, 1981. [Erratum: Nucl.Phys.B 213, 545 (1983)].
[22] Daniel de Florian and Massimiliano Grazzini. The Back-to-back region in e+ e- energy-energy correlation. *Nucl. Phys. B*, 704:387–403, 2005.
[23] Ian Moult and Hua Xing Zhu. Simplicity from Recoil: The Three-Loop Soft Function and Factorization for the Energy-Energy Correlation. *JHEP*, 08:160, 2018.
[24] Carlota Andres, Fabio Dominguez, Raghav Kunnawalkam Elayavalli, Jack Holguin, Cyrille Marquet, and Ian Moult. Resolving the Scales of the Quark-Gluon Plasma with Energy Correlators. *Phys. Rev. Lett.*, 130(26):262301, 2023.
[25] Hannah Bossi, Austin Baty, Yi Chen, Yu-Chen (Janice) Chen, Gian-Michele Innocenti, Marcello Maggi, Chris McGinn, and Yen-Jie Lee. Measurement of the energy-energy correlator in the back-to-back limit using the archived ALEPH e+e- data at 91.2 GeV. *PoS*, LHCP2024:228, 2025.
[26] Carlota Andres, Fabio Dominguez, Jack Holguin, Cyrille Marquet, and Ian Moult. Towards an interpretation of the first measurements of energy correlators in the quark-gluon plasma. *JHEP*, 03:166, 2025.
[27] João Barata, Zhong-Bo Kang, Xoán Mayo López, and Jani Penttala. Energy-Energy Correlator for Jet Production in pp and pA Collisions. *Phys. Rev. Lett.*, 134(25):251903, 2025.
[28] Aram Hayrapetyan et al. Measurement of Energy Correlators inside Jets and Determination of the Strong Coupling αS(mZ). *Phys. Rev. Lett.*, 133(7):071903, 2024.
[29] Xiaohui Liu and Hua Xing Zhu. Nucleon Energy Correlators. *Phys. Rev. Lett.*, 130(9):091901, 2023.
[30] Hao-Yu Liu, Xiaohui Liu, Ji-Chen Pan, Feng Yuan, and Hua Xing Zhu. Nucleon Energy Correlators for the Color Glass Condensate. *Phys. Rev. Lett.*, 130(18):181901, 2023.
[31] Haotian Cao, Xiaohui Liu, and Hua Xing Zhu. Toward precision measurements of nucleon energy correlators in lepton-nucleon collisions. *Phys. Rev. D*, 107(11):114008, 2023.
[32] Haotian Cao, Hai Tao Li, and Zihao Mi. Bjorken x weighted energy-energy correlators from the target fragmentation region to the current fragmentation region. *Phys. Rev. D*, 109(9):096004, 2024.
[33] Jun Gao, Hai Tao Li, and Yu Jiao Zhu. Energy correlators resolving proton spin. *Phys. Rev. D*, 113(3):034028, 2026.
[34] Heikki Mäntysaari, Yossathorn Tawabutr, and Xuan-Bo Tong. Nucleon energy correlators for the odderon. *Phys. Rev. D*, 112(11):114027, 2025.
[35] Xiaohui Liu and Hua Xing Zhu. TMDs from Semi-inclusive Energy Correlators. 3 2024.
[36] Yu Jiao Zhu. Energy correlators in semi-inclusive electron-positron annihilation. *Phys. Rev. D*, 113(1):014025, 2026.

[37] Qing-Hong Cao, Zhite Yu, C. P. Yuan, Shutao Zhang, and Hua Xing Zhu. Collins-type fragmentation energy correlator in semi-inclusive deep inelastic lepton-hadron scattering. *JHEP*, 02:244, 2026.

[38] Pedro Cal, Felix Ringer, and Wouter J. Waalewijn. The jet shape at NLL'. *JHEP*, 05:143, 2019.

[39] Marc Riembau and Minho Son. Flow between Extremal One-Point Energy Correlators in QCD. *Phys. Rev. Lett.*, 136(10):101901, 2026.

[40] Zihao Mi and Zhan Wang. One-point energy correlator inside jets. *JHEP*, 11:090, 2025.

[41] Mei-Sen Gao, Zhong-Bo Kang, Wanchen Li, and Ding Yu Shao. Accessing Nucleon Transversity with One-Point Energy Correlators. *Phys. Rev. Lett.*, 136(15):151902, 2026.

[42] Yu-Kun Song, Shu-Yi Wei, Lei Yang, and Jian Zhou. Gluon Polarimetry with Energy-Energy Correlators. *Phys. Rev. Lett.*, 136(13):131901, 2026.

[43] Yu Fu, Zhong-Bo Kang, Jani Penttala, and Yiyu Zhou. Exploring nuclear modification using one-point energy correlator at the electron-ion collider. 12 2025.

[44] Energy Correlators Within Jets in Transversely Polarized Proton-Proton Collisions at $\sqrt{s} = 200$ GeV. 4 2026.

[45] Zhong-Bo Kang, Robert Kao, Meijian Li, and Jani Penttala. One-point energy correlator for deep inelastic scattering at small x. 3 2026.

[46] Ahmed Ali, E. Pietarinen, and W. James Stirling. Transverse Energy-energy Correlations: A Test of Perturbative QCD for the Proton - Anti-proton Collider. *Phys. Lett. B*, 141:447–454, 1984.

[47] Ahmed Ali, Fernando Barreiro, Javier Llorente, and Wei Wang. Transverse Energy-Energy Correlations in Next-to-Leading Order in α_s at the LHC. *Phys. Rev. D*, 86:114017, 2012.

[48] AnJie Gao, Hai Tao Li, Ian Moult, and Hua Xing Zhu. Precision QCD Event Shapes at Hadron Colliders: The Transverse Energy-Energy Correlator in the Back-to-Back Limit. *Phys. Rev. Lett.*, 123(6):062001, 2019.

[49] Hai Tao Li, Ivan Vitev, and Yu Jiao Zhu. Transverse-Energy-Energy Correlations in Deep Inelastic Scattering. *JHEP*, 11:051, 2020.

[50] Ahmed Ali, Gang Li, Wei Wang, and Zhi-Peng Xing. Transverse energy–energy correlations of jets in the electron–proton deep inelastic scattering at HERA. *Eur. Phys. J. C*, 80(12):1096, 2020.

[51] Anjie Gao, Hai Tao Li, Ian Moult, and Hua Xing Zhu. The transverse energy-energy correlator at next-to-next-to-next-to-leading logarithm. *JHEP*, 09:072, 2024.

[52] Shohini Bhattacharya, Zhong-Bo Kang, Diego Padilla, and Jani Penttala. Probing the Sivers Asymmetry with Transverse Energy-Energy Correlators in the Small-x Regime. 4 2025.

[53] George F. Sterman. Jet Structure in e+ e- Annihilation with Massless Hadrons. 12 1975.

[54] João Barata and Swagato Mukherjee. Probing celestial energy and charge correlations through real-time quantum simulations: Insights from the Schwinger model. *Phys. Rev. D*, 111(3):L031901, 2025.

[55] Kyle Lee, Francesco Turro, and Xiaojun Yao. Quantum computing for energy correlators. *Phys. Rev. D*, 111(5):054514, 2025.

[56] Qing-Hong Cao, Ying-Ying Li, Xiaohui Liu, Liang-Qi Zhang, and Ke Zhao. Exponentially improved quantum simulation of scalar QFT. 4 2026.

[57] Hao Chen, Ian Moult, XiaoYuan Zhang, and Hua Xing Zhu. Rethinking jets with energy correlators: Tracks, resummation, and analytic continuation. *Phys. Rev. D*, 102(5):054012, 2020.

[58] Hao Chen, Ian Moult, Jesse Thaler, and Hua Xing Zhu. Non-Gaussianities in collider energy flux. *JHEP*, 07:146, 2022.

[59] Wen Chen, Jun Gao, Yibei Li, Zhen Xu, Xiaoyuan Zhang, and Hua Xing Zhu. NNLL resummation for projected three-point energy correlator. *JHEP*, 05:043, 2024.

[60] Lin Dai, Chul Kim, and Adam K. Leibovich. Large N-point energy correlator in the collinear limit. *Phys. Rev. D*, 112(9):094015, 2025.

[61] Ankita Budhraja, Hao Chen, and Wouter J. Waalewijn. ν-point energy correletors with FastEEC: Small-x physics from LHC jets. *Phys. Lett. B*, 861:139239, 2025.

[62] Ankita Budhraja and Wouter J. Waalewijn. FastEEC: Fast evaluation of N-point energy correlators. *Phys. Lett. B*, 861:139276, 2025.

[63] Yi-Lin Wang, Jun Gao, Ying-Ying Li, and Huaxing Zhu. Parton spin correlations and $\mathcal{CP}$ properties in Higgs boson decay at future lepton colliders. 1 2026.

[64] Ankita Budhraja, Isabelle Pels, and Wouter J. Waalewijn. Higher-point Energy Correlators: Factorization in the Back-to-Back Limit & Non-perturbative Effects. 3 2026.

[65] Evan Craft, Kyle Lee, Bianka Meçaj, and Ian Moult. Beautiful and Charming Energy Correlators. 10 2022.

[66] Max Jaarsma, Yibei Li, Ian Moult, Wouter J. Waalewijn, and Hua Xing Zhu. Energy correlators on tracks: resummation and non-perturbative effects. *JHEP*, 12:087, 2023.

[67] Kyle Lee and Ian Moult. Energy Correlators Taking Charge. 8 2023.

[68] Kyle Lee and Ian Moult. Joint Track Functions: Expanding the Space of Calculable Correlations at Colliders. 8 2023.

[69] Pier Francesco Monni, Gherardo Vita, Zhen Xu, and Hua Xing Zhu. On the Edge of Safety: Charge-Charge Correlation in the Back-to-Back Limit. 8 2025.

[70] Zhong-Bo Kang, Kyle Lee, Ding Yu Shao, and Fanyi Zhao. Probing transverse momentum dependent structures with azimuthal dependence of energy correlators. *JHEP*, 03:153, 2024.

[71] Zoltán Tulipánt, Adam Kardos, and Gábor Somogyi. Energy–energy correlation in electron–positron annihilation at NNLL + NNLO accuracy. *Eur. Phys. J. C*, 77(11):749, 2017.

[72] Lance J. Dixon, Ming-Xing Luo, Vladyslav Shtabovenko, Tong-Zhi Yang, and Hua Xing Zhu. Analytical Computation of Energy-Energy Correlation at Next-to-Leading Order in QCD. *Phys. Rev. Lett.*, 120(10):102001, 2018.

[73] Zhu-Yu Ren, Sheng-Quan Wang, Jian-Ming Shen, Xing-Gang Wu, Leonardo Di Giustino, Philip G. Ratcliffe, and Stanley J. Brodsky. Novel analysis for the energy-energy correlation in electron-positron annihilation in the perturbative domain. 4 2026.

[74] Zhong-Bo Kang, Jani Penttala, and Congyue Zhang. Determination of the strong coupling constant and the Collins-Soper kernel from the energy-energy correlator in e^+e^- collisions. 10 2024.

[75] Alejandro Bris Cuerpo, Ignazio Scimemi, and Alexey Vladimirov. Assessing the sensitivity of energy-energy correlations in e^+e^- annihilation to TMD dynamics. *JHEP*, 11:013, 2025.

[76] Ignazio Scimemi and Alexey Vladimirov. Non-perturbative structure of semi-inclusive deep-inelastic and Drell-Yan scattering at small transverse momentum. *JHEP*, 06:137, 2020.

[77] Peng Sun, Joshua Isaacson, C. P. Yuan, and Feng Yuan. Nonperturbative functions for SIDIS and Drell–Yan processes. *Int. J. Mod. Phys. A*, 33(11):1841006, 2018.

[78] Valentin Moos, Ignazio Scimemi, Alexey Vladimirov, and Pia Zurita. Extraction of unpolarized transverse momentum distributions from the fit of Drell-Yan data at N^{4}LL. *JHEP*, 05:036, 2024.

[79] Alessandro Bacchetta, Valerio Bertone, Chiara Bissolotti, Giuseppe Bozzi, Matteo Cerutti, Filippo Delcarro, Marco Radici, Lorenzo Rossi, and Andrea Signori. Flavor dependence of unpolarized quark transverse momentum distributions from a global fit. *JHEP*, 08:232, 2024.

[80] Artur Avkhadiev, Phiala E. Shanahan, Michael L. Wagman, and Yong Zhao. Determination of the Collins-Soper Kernel from Lattice QCD. *Phys. Rev. Lett.*, 132(23):231901, 2024.

[81] Dennis Bollweg, Xiang Gao, Swagato Mukherjee, and Yong Zhao. Nonperturbative Collins-Soper kernel from chiral quarks with physical masses. *Phys. Lett. B*, 852:138617, 2024.

[82] Min-Huan Chu et al. Lattice calculation of the intrinsic soft function and the Collins-Soper kernel. *JHEP*, 08:172, 2023.

[83] Artur Avkhadiev, Valerio Bertone, Chiara Bissolotti, Matteo Cerutti, Yang Fu, Simone Rodini, Phiala Shanahan, Michael Wagman, and Yong Zhao. An extraction of the Collins-Soper kernel from a joint analysis of experimental and lattice data. 10 2025.

[84] Ugo Giuseppe Aglietti, Giancarlo Ferrera, and Lorenzo Rossi. A global analysis of Energy-Energy Correlation data: determination of α_S and non-perturbative QCD parameters. 3 2026.

[85] Stella T. Schindler, Iain W. Stewart, and Zhiquan Sun. Renormalons in the energy-energy correlator. *JHEP*, 10:187, 2023. [Erratum: JHEP 10, 175 (2024)].

[86] Gregory P. Korchemsky and George F. Sterman. Power corrections to event shapes and factorization. *Nucl. Phys. B*, 555:335–351, 1999.

[87] Andrei V. Belitsky, G. P. Korchemsky, and George F. Sterman. Energy flow in QCD and event shape functions. *Phys. Lett. B*, 515:297–307, 2001.

[88] Carola F. Berger, Tibor Kucs, and George F. Sterman. Event shape / energy flow correlations. *Phys. Rev. D*, 68:014012, 2003.

[89] Christopher Lee and George F. Sterman. Momentum Flow Correlations from Event Shapes: Factorized Soft Gluons and Soft-Collinear Effective Theory. *Phys. Rev. D*, 75:014022, 2007.

[90] Thomas Becher and Guido Bell. Enhanced nonperturbative effects through the collinear anomaly. *Phys. Rev. Lett.*, 112(18):182002, 2014.

[91] Kyle Lee, Aditya Pathak, Iain W. Stewart, and Zhiquan Sun. Nonperturbative Effects in Energy Correlators: From Characterizing Confinement Transition to Improving αs Extraction. *Phys. Rev. Lett.*, 133(23):231902, 2024.

[92] Hao Chen, Pier Francesco Monni, Zhen Xu, and Hua Xing Zhu. Scaling Violation in Power Corrections to Energy Correlators from the Light-Ray Operator Product Expansion. *Phys. Rev. Lett.*, 133(23):231901, 2024.

[93] Cyuan-Han Chang, Hao Chen, David Simmons-Duffin, and Hua Xing Zhu. Seeing through the confinement screen: DGLAP/BFKL mixing and light-ray matching in QCD. *JHEP*, 02:251, 2026.

[94] Hao Chen, Ian Moult, and Hua Xing Zhu. Quantum Interference in Jet Substructure from Spinning Gluons. *Phys. Rev. Lett.*, 126(11):112003, 2021.

[95] Hao Chen, Ian Moult, and Hua Xing Zhu. Spinning gluons from the QCD light-ray OPE. *JHEP*, 08:233, 2022.

[96] Hao Chen and Yibei Li. Operator structure of power corrections and anomalous scaling in energy correlators. 4 2026.

[97] Chuan-Qi He, Hongxi Xing, Tong-Zhi Yang, and Hua Xing Zhu. Single-Inclusive Hadron Production in Electron-Positron Annihilation at Next-to-Next-to-Next-to-Leading Order in QCD. *Phys. Rev. Lett.*, 135(10):101901, 2025.

[98] Liang Dong, Shen Fang, Jun Gao, Hai Tao Li, Ding Yu Shao, Hua Xing Zhu, and Yu Jiao Zhu. Two-Dimensional Transverse-Momentum Subtraction and Semi-Inclusive Deep-Inelastic Scattering at N^3LO in QCD. 3 2026.

[99] Michał Czakon, Terry Generet, Alexander Mitov, and Rene Poncelet. Identified Hadron Production at Hadron Colliders in Next-to-Next-to-Leading-Order QCD. *Phys. Rev. Lett.*, 135(17):17, 2025.

[100] Thomas Gehrmann, Andreas von Manteuffel, Vasily Sotnikov, and Tongzhi Yang. The four-loop non-singlet splitting functions in QCD. 4 2026.

[101] Xiao Lin Li, Xiaohui Liu, Feng Yuan, and Hua Xing Zhu. Illuminating nucleon-gluon interference via calorimetric asymmetry. *Phys. Rev. D*, 108(9):L091502, 2023.

[102] Megan Connors, Christine Nattrass, Rosi Reed, and Sevil Salur. Jet measurements in heavy ion physics. *Rev. Mod. Phys.*, 90:025005, 2018.

[103] Wit Busza, Krishna Rajagopal, and Wilke van der Schee. Heavy Ion Collisions: The Big Picture, and the Big Questions. *Ann. Rev. Nucl. Part. Sci.*, 68:339–376, 2018.

[104] Leticia Cunqueiro and Anne M. Sickles. Studying the QGP with Jets at the LHC and RHIC. *Prog. Part. Nucl. Phys.*, 124:103940, 2022.

[105] Liliana Apolinário, Yen-Jie Lee, and Michael Winn. Heavy quarks and jets as probes of the QGP. *Prog. Part. Nucl. Phys.*, 127:103990, 2022.

[106] Vladimir Chekhovsky et al. Observation of nuclear modification of energy-energy correlators inside jets in heavy ion collisions. *Phys. Lett. B*, 866:139556, 2025.

[107] R. Baier, Yuri L. Dokshitzer, Alfred H. Mueller, S. Peigne, and D. Schiff. Radiative energy loss of high-energy quarks and gluons in a finite volume quark - gluon plasma. *Nucl. Phys. B*, 483:291–320, 1997.

[108] R. Baier, Yuri L. Dokshitzer, Alfred H. Mueller, S. Peigne, and D. Schiff. Radiative energy loss and p(T) broadening of high-energy partons in nuclei. *Nucl. Phys. B*, 484:265–282, 1997.

[109] B. G. Zakharov. Fully quantum treatment of the Landau-Pomeranchuk-Migdal effect in QED and QCD. *JETP Lett.*, 63:952–957, 1996.

[110] B. G. Zakharov. Radiative energy loss of high-energy quarks in finite size nuclear matter and quark - gluon plasma. *JETP Lett.*, 65:615–620, 1997.

[111] Fabio Domínguez, Jose Guilherme Milhano, Carlos A. Salgado, Konrad Tywoniuk, and Víctor Vila. Mapping collinear in-medium parton splittings. *Eur. Phys. J. C*, 80(1):11, 2020.

[112] Johannes Hamre Isaksen and Konrad Tywoniuk. Wilson line correlators beyond the large-N_c. *JHEP*, 21:125, 2020.

[113] Carlota Andres, Fabio Dominguez, Jack Holguin, Cyrille Marquet, and Ian Moult. A coherent view of the quark-gluon plasma from energy correlators. *JHEP*, 09:088, 2023.

[114] Carlota Andres, Fabio Dominguez, Jack Holguin, Cyrille Marquet, and Ian Moult. Seeing beauty in the quark-gluon plasma with energy correlators. *Phys. Rev. D*, 110(3):L031503, 2024.

[115] Carlota Andres, Jack Holguin, Raghav Kunnawalkam Elayavalli, and Jussi Viinikainen. Minimizing Selection Bias in Inclusive Jets in Heavy-Ion Collisions with Energy Correlators. *Phys. Rev. Lett.*, 134(8):082303, 2025.

[116] Carlota Andres and Jack Holguin. Minimizing Selection Bias in Inclusive Jets in Heavy-Ion Collisions with Energy Correlators – arXiv note. 9 2024.

[117] Wei Chen, Shanshan Cao, Tan Luo, Long-Gang Pang, and Xin-Nian Wang. Effects of jet-induced medium excitation in γ-hadron correlation in A+A collisions. *Phys. Lett. B*, 777:86–90, 2018.

[118] Wei Chen, Shanshan Cao, Tan Luo, Long-Gang Pang, and Xin-Nian Wang. Medium modification of γ-jet fragmentation functions in Pb+Pb collisions at LHC. *Phys. Lett. B*, 810:135783, 2020.

[119] Wenbin Zhao, Weiyao Ke, Wei Chen, Tan Luo, and Xin-Nian Wang. From Hydrodynamics to Jet Quenching, Coalescence, and Hadron Cascade: A Coupled Approach to Solving the RAA⊗v2 Puzzle. *Phys. Rev. Lett.*, 128(2):022302, 2022.

[120] Hanlin Li, Fuming Liu, Guo-liang Ma, Xin-Nian Wang, and Yan Zhu. Mach cone induced by γ-triggered jets in high-energy heavy-ion collisions. *Phys. Rev. Lett.*, 106:012301, 2011.

[121] Yayun He, Tan Luo, Xin-Nian Wang, and Yan Zhu. Linear Boltzmann Transport for Jet Propagation in the Quark-Gluon Plasma: Elastic Processes and Medium Recoil. *Phys. Rev. C*, 91:054908, 2015. [Erratum: Phys.Rev.C 97, 019902 (2018)].

[122] Shanshan Cao, Tan Luo, Guang-You Qin, and Xin-Nian Wang. Linearized Boltzmann transport model for jet propagation in the quark-gluon plasma: Heavy quark evolution. *Phys. Rev. C*, 94(1):014909, 2016.

[123] Tan Luo, Yayun He, Shanshan Cao, and Xin-Nian Wang. Linear Boltzmann transport for jet propagation in the quark-gluon plasma: Inelastic processes and jet modification. *Phys. Rev. C*, 109(3):034919, 2024.

[124] Xiao-feng Guo and Xin-Nian Wang. Multiple scattering, parton energy loss and modified fragmentation functions in deeply inelastic e A scattering. *Phys. Rev. Lett.*, 85:3591–3594, 2000.

[125] Xin-Nian Wang and Xiao-feng Guo. Multiple parton scattering in nuclei: Parton energy loss. *Nucl. Phys. A*, 696:788–832, 2001.

[126] Longgang Pang, Qun Wang, and Xin-Nian Wang. Effects of initial flow velocity fluctuation in event-by-event (3+1)D hydrodynamics. *Phys. Rev. C*, 86:024911, 2012.

[127] Long-Gang Pang, Yoshitaka Hatta, Xin-Nian Wang, and Bo-Wen Xiao. Analytical and numerical Gubser solutions of the second-order hydrodynamics. *Phys. Rev. D*, 91(7):074027, 2015.

[128] Long-Gang Pang, Hannah Petersen, and Xin-Nian Wang. Pseudorapidity distribution and decorrelation of anisotropic flow within the open-computing-language implementation CLVisc hydrodynamics. *Phys. Rev. C*, 97(6):064918, 2018.

[129] Wei Chen, Zhong Yang, Yayun He, Weiyao Ke, Longgang Pang, and Xin-Nian Wang. Search for the Elusive Jet-Induced Diffusion Wake in Z/γ-Jets with 2D Jet Tomography in High-Energy Heavy-Ion Collisions. *Phys. Rev. Lett.*, 127(8):082301, 2021.

[130] Zhong Yang, Tan Luo, Wei Chen, Long-Gang Pang, and Xin-Nian Wang. 3D Structure of Jet-Induced Diffusion Wake in an Expanding Quark-Gluon Plasma. *Phys. Rev. Lett.*, 130(5):052301, 2023.

[131] Zhong Yang, Yayun He, Ian Moult, and Xin-Nian Wang. Probing the Short-Distance Structure of the Quark-Gluon Plasma with Energy Correlators. *Phys. Rev. Lett.*, 132(1):011901, 2024.

[132] Yuri L. Dokshitzer, Valery A. Khoze, and S. I. Troian. On specific QCD properties of heavy quark fragmentation ('dead cone'). *J. Phys. G*, 17:1602–1604, 1991.

[133] Nestor Armesto, Carlos A. Salgado, and Urs Achim Wiedemann. Medium induced gluon radiation off massive quarks fills the dead cone. *Phys. Rev. D*, 69:114003, 2004.

[134] R. Thomas, Burkhard Kampfer, and G. Soff. Gluon emission of heavy quarks: Dead cone effect. *Acta Phys. Hung. A*, 22:83–91, 2005.

[135] Wen-Jing Xing, Shanshan Cao, Guang-You Qin, and Xin-Nian Wang. Flavor Hierarchy of Jet Energy Correlators inside the Quark-Gluon Plasma. *Phys. Rev. Lett.*, 134(5):052301, 2025.

[136] Liliana Apolinário, Raghav Kunnawalkam Elayavalli, Nuno Olavo Madureira, Jun-Xing Sheng, Xin-Nian Wang, and Zhong Yang. Flavor dependence of energy-energy correlators. *Phys. Rev. D*, 112(5):054018, 2025.

[137] Shreyasi Acharya et al. Energy-energy correlators in charm-tagged jets in proton-proton collisions at $\sqrt{s} = \mathbf{13}$ TeV. 4 2025.

[138] Hannah Bossi, Arjun Srinivasan Kudinoor, Ian Moult, Daniel Pablos, Ananya Rai, and Krishna Rajagopal. Imaging the wakes of jets with energy-energy-energy correlators. *JHEP*, 12:073, 2024.

[139] Hannah Bossi, Arjun Kudinoor, Ian Moult, Daniel Pablos, Ananya Rai, and Krishna Rajagopal. Imaging the jet-induced medium response with energy correlators. *EPJ Web Conf.*, 364:10001, 2026.

[140] João Barata, Matvey V. Kuzmin, José Guilherme Milhano, and Andrey V. Sadofyev. Giving wake to energy-energy correlators: Hydrodynamic response on the celestial sphere. *Phys. Rev. D*, 112(1):016005, 2025.

[141] João Barata, Ian Moult, Andrey V. Sadofyev, and João M. Silva. Dissecting Jet Modification in the QGP with Multi-Point Energy Correlators. 3 2025.

[142] João Barata, Matvey V. Kuzmin, Ian Moult, Andrey V. Sadofyev, and João M. Silva. Hydrodynamics and Energy Correlators. 4 2026.

[143] João Barata, José Guilherme Milhano, and Andrey V. Sadofyev. Picturing QCD jets in anisotropic matter: from jet shapes to energy energy correlators. *Eur. Phys. J. C*, 84(2):174, 2024.

[144] João Barata, Paul Caucal, Alba Soto-Ontoso, and Robert Szafron. Advancing the understanding of energy-energy correlators in heavy-ion collisions. *JHEP*, 11:060, 2024.

[145] João Barata and Robert Szafron. Leading order track functions in a hot and dense QGP. *Phys. Rev. D*, 110(3):L031501, 2024.

[146] Balbeer Singh and Varun Vaidya. Factorization for energy-energy correlator in heavy ion collision. *JHEP*, 06:071, 2025.

[147] João Barata, Ian Moult, and João M. Silva. Tracking Energy Loss in Heavy Ion Collisions. 9 2024.

[148] John C. Collins, Davison E. Soper, and George F. Sterman. Factorization for Short Distance Hadron - Hadron Scattering. *Nucl. Phys. B*, 261:104–142, 1985.

[149] John C. Collins, Davison E. Soper, and George F. Sterman. Factorization of Hard Processes in QCD. *Adv. Ser. Direct. High Energy Phys.*, 5:1–91, 1989.

[150] H. David Politzer. Power Corrections at Short Distances. *Nucl. Phys. B*, 172:349–382, 1980.

[151] R. L. Jaffe and M. Soldate. Twist Four in the QCD Analysis of Leptoproduction. *Phys. Lett. B*, 105:467–472, 1981.

[152] R. Keith Ellis, W. Furmanski, and R. Petronzio. Unraveling Higher Twists. *Nucl. Phys. B*, 212:29, 1983.

[153] R. Keith Ellis, W. Furmanski, and R. Petronzio. Power Corrections to the Parton Model in QCD. *Nucl. Phys. B*, 207:1–14, 1982.

[154] R. L. Jaffe and M. Soldate. Twist Four in Electroproduction: Canonical Operators and Coefficient Functions. *Phys. Rev. D*, 26:49–68, 1982.

[155] R. L. Jaffe. Parton Distribution Functions for Twist Four. *Nucl. Phys. B*, 229:205–230, 1983.

[156] Jian-wei Qiu and George F. Sterman. Power corrections to hadronic scattering. 2. Factorization. *Nucl. Phys. B*, 353:137–164, 1991.

[157] Jian-wei Qiu and George F. Sterman. Power corrections in hadronic scattering. 1. Leading 1/Q**2 corrections to the Drell-Yan cross-section. *Nucl. Phys. B*, 353:105–136, 1991.

[158] Ma Luo, Jian-wei Qiu, and George F. Sterman. Higher twist effects in hadronic scattering. In *Particles & Fields 91: Meeting of the Division of Particles & Fields of the APS*, pages 0633–636, 8 1991.

[159] M. Luo, Jian-wei Qiu, and George F. Sterman. Cronin effect in photoproduction and deeply inelastic scattering. In *7th Meeting of the APS Division of Particles Fields*, pages 951–953, 11 1992.

[160] Ma Luo, Jian-wei Qiu, and George F. Sterman. Nuclear dependence at large transverse momentum. *Phys. Lett. B*, 279:377–383, 1992.

[161] Ma Luo, Jian-wei Qiu, and George F. Sterman. Twist four nuclear parton distributions from photoproduction. *Phys. Rev. D*, 49:4493–4502, 1994.

[162] M. Luo, Jian-wei Qiu, and George F. Sterman. Anomalous nuclear enhancement in deeply inelastic scattering and photoproduction. *Phys. Rev. D*, 50:1951–1971, 1994.

[163] Kyle Devereaux, Wenqing Fan, Weiyao Ke, Kyle Lee, and Ian Moult. Probing cold nuclear matter with energy correlators. *Phys. Rev. C*, 112(3):035202, 2025.

[164] Yu Fu, Berndt Müller, and Chathuranga Sirimanna. Modification of the Jet Energy-Energy Correlator in Cold Nuclear Matter. *Phys. Rev. Lett.*, 135(11):112302, 2025.

[165] Carlota Andres, Fabio Dominguez, Jack Holguin, Cyrille Marquet, and Ian Moult. Simple Scaling Laws for Energy Correlators in Nuclear Matter. *Phys. Rev. Lett.*, 136(12):122301, 2026.

[166] Weiyao Ke, Bianka Mecaj, and Ivan Vitev. Renormalization group evolution for in-medium energy correlators. *JHEP*, 04:155, 2026.

[167] Christian W. Bauer, Sean Fleming, and Michael E. Luke. Summing Sudakov logarithms in $B \to X_s\gamma$in effective field theory. *Phys. Rev. D*, 63:014006, 2000.

[168] Christian W. Bauer, Sean Fleming, Dan Pirjol, and Iain W. Stewart. An Effective field theory for collinear and soft gluons: Heavy to light decays. *Phys. Rev. D*, 63:114020, 2001.

[169] Christian W. Bauer and Iain W. Stewart. Invariant operators in collinear effective theory. *Phys. Lett. B*, 516:134–142, 2001.

[170] Christian W. Bauer, Dan Pirjol, and Iain W. Stewart. Soft collinear factorization in effective field theory. *Phys. Rev. D*, 65:054022, 2002.

[171] Christian W. Bauer, Sean Fleming, Dan Pirjol, Ira Z. Rothstein, and Iain W. Stewart. Hard scattering factorization from effective field theory. *Phys. Rev. D*, 66:014017, 2002.

[172] Grigory Ovanesyan and Ivan Vitev. An effective theory for jet propagation in dense QCD matter: jet broadening and medium-induced bremsstrahlung. *JHEP*, 06:080, 2011.

[173] Grigory Ovanesyan and Ivan Vitev. Medium-induced parton splitting kernels from Soft Collinear Effective Theory with Glauber gluons. *Phys. Lett. B*, 706:371–378, 2012.

[174] Pi Duan, Weiyao Ke, Guang-You Qin, and Lei Wang. Uncover the correlation between jet energy correlators and multiplicity fluctuations. 4 2026.

[175] Zhong-Bo Kang, Jani Penttala, Fanyi Zhao, and Yiyu Zhou. Transverse energy-energy correlators in the color-glass condensate at the electron-ion collider. *Phys. Rev. D*, 109(9):094012, 2024.

[176] Zhong-Bo Kang, Sookhyun Lee, Jani Penttala, Fanyi Zhao, and Yiyu Zhou. Transverse energy-energy correlator for vector boson-tagged hadron production in pp and pA collisions. *Phys. Rev. D*, 112(1):014012, 2025.

[177] Zhong-Bo Kang, Robert Kao, Meijian Li, and Jani Penttala. Transverse energy-energy correlators at small x for photon-hadron production. *Phys. Rev. D*, 112(7):076006, 2025.

[178] Kai-Bao Chen, Jian-Ping Ma, and Xuan-Bo Tong. The connection between nucleon energy correlators and fracture functions. *JHEP*, 08:227, 2024.

[179] Yingsheng Huang, Xuan-Bo Tong, and Hao-Lin Wang. Nucleon Energy Correlators as a Probe of Light-Quark Dipole Operators at the Electron-Ion Collider. *Phys. Rev. Lett.*, 136(13):131902, 2026.

[180] L. Trentadue and G. Veneziano. Fracture functions: An Improved description of inclusive hard processes in QCD. *Phys. Lett. B*, 323:201–211, 1994.

[181] Yoshitaka Hatta, Bo-Wen Xiao, Feng Yuan, and Jian Zhou. Anisotropy in Dijet Production in Exclusive and Inclusive Processes. *Phys. Rev. Lett.*, 126(14):142001, 2021.

[182] Yuxun Guo, Xiaohui Liu, Feng Yuan, and Hua Xing Zhu. Long-Range Azimuthal Correlation, Entanglement, and Bell Inequality Violation by Spinning Gluons at the Large Hadron Collider. *Research*, 2025:0552, 2025.

[183] Vincenzo Barone, Stefano Melis, and Alexei Prokudin. The Boer-Mulders effect in unpolarized SIDIS: An Analysis of the COMPASS and HERMES data on the cos 2 phi asymmetry. *Phys. Rev. D*, 81:114026, 2010.

[184] E. Christova, D. Kotlorz, and E. Leader. New study of the Boer-Mulders function: Implications for the quark and hadron transverse momenta. *Phys. Rev. D*, 102(1):014035, 2020.

[185] Bing Zhang, Zhun Lu, Bo-Qiang Ma, and Ivan Schmidt. cos(2phi) asymmetries in unpolarized semi-inclusive DIS. *Phys. Rev. D*, 78:034035, 2008.

[186] Radja Boughezal, Emanuele Mereghetti, and Frank Petriello. Dilepton production in the SMEFT at O(1/Λ4). *Phys. Rev. D*, 104(9):095022, 2021.

[187] Xin-Kai Wen, Bin Yan, Zhite Yu, and C. P. Yuan. Dihadron azimuthal asymmetry and light-quark dipole moments at the Electron-Ion Collider. 8 2024.

[188] An-Ping Chen, Xiaohui Liu, and Yan-Qing Ma. Shedding Light on Hadronization by Quarkonium Energy Correlator. *Phys. Rev. Lett.*, 133:19, 2024.

[189] Alexander Zhiboedov. On Conformal Field Theories With Extremal a/c Values. *JHEP*, 04:038, 2014.

[190] Marc Riembau and Minho Son. One-point correlators of conserved and nonconserved charges in QCD. *Phys. Rev. D*, 111(1):014004, 2025.

[191] M. Ablikim et al. Future Physics Programme of BESIII. *Chin. Phys. C*, 44(4):040001, 2020.

[192] M. Achasov et al. STCF conceptual design report (Volume 1): Physics & detector. *Front. Phys. (Beijing)*, 19(1):14701, 2024.

[193] Jonathan M. Butterworth, Adam R. Davison, Mathieu Rubin, and Gavin P. Salam. Jet substructure as a new Higgs search channel at the LHC. *Phys. Rev. Lett.*, 100:242001, 2008.

[194] Stephen D. Ellis, Christopher K. Vermilion, and Jonathan R. Walsh. Recombination Algorithms and Jet Substructure: Pruning as a Tool for Heavy Particle Searches. *Phys. Rev. D*, 81:094023, 2010.

[195] David Krohn, Jesse Thaler, and Lian-Tao Wang. Jet Trimming. *JHEP*, 02:084, 2010.

[196] Jesse Thaler and Ken Van Tilburg. Identifying Boosted Objects with N-subjettiness. *JHEP*, 03:015, 2011.

[197] Jesse Thaler and Ken Van Tilburg. Maximizing Boosted Top Identification by Minimizing N-subjettiness. *JHEP*, 02:093, 2012.

[198] Andrew J. Larkoski, Gavin P. Salam, and Jesse Thaler. Energy Correlation Functions for Jet Substructure. *JHEP*, 06:108, 2013.

[199] Andrew J. Larkoski, Simone Marzani, Gregory Soyez, and Jesse Thaler. Soft Drop. *JHEP*, 05:146, 2014.

[200] Yibei Li, Ian Moult, Solange Schrijnder van Velzen, Wouter J. Waalewijn, and Hua Xing Zhu. Extending Precision Perturbative QCD with Track Functions. *Phys. Rev. Lett.*, 128(18):182001, 2022.

[201] Duff Neill, Andreas Papaefstathiou, Wouter J. Waalewijn, and Lorenzo Zoppi. Phenomenology with a recoil-free jet axis: TMD fragmentation and the jet shape. *JHEP*, 01:067, 2019.

[202] Feng Yuan. Azimuthal asymmetric distribution of hadrons inside a jet at hadron collider. *Phys. Rev. Lett.*, 100:032003, 2008.

[203] Massimiliano Procura and Iain W. Stewart. Quark Fragmentation within an Identified Jet. *Phys. Rev. D*, 81:074009, 2010. [Erratum: Phys.Rev.D 83, 039902 (2011)].

[204] Ambar Jain, Massimiliano Procura, and Wouter J. Waalewijn. Parton Fragmentation within an Identified Jet at NNLL. *JHEP*, 05:035, 2011.

[205] Reggie Bain, Yiannis Makris, and Thomas Mehen. Transverse Momentum Dependent Fragmenting Jet Functions with Applications to Quarkonium Production. *JHEP*, 11:144, 2016.

[206] Duff Neill, Ignazio Scimemi, and Wouter J. Waalewijn. Jet axes and universal transverse-momentum-dependent fragmentation. *JHEP*, 04:020, 2017.

[207] Zhong-Bo Kang, Xiaohui Liu, Felix Ringer, and Hongxi Xing. The transverse momentum distribution of hadrons within jets. *JHEP*, 11:068, 2017.

[208] Zhong-Bo Kang, Kyle Lee, and Fanyi Zhao. Polarized jet fragmentation functions. *Phys. Lett. B*, 809:135756, 2020.

[209] Umberto D'Alesio, Francesco Murgia, and Cristian Pisano. Azimuthal asymmetries for hadron distributions inside a jet in hadronic collisions. *Phys. Rev. D*, 83:034021, 2011.

[210] Zhong-Bo Kang, Alexei Prokudin, Felix Ringer, and Feng Yuan. Collins azimuthal asymmetries of hadron production inside jets. *Phys. Lett. B*, 774:635–642, 2017.

[211] Umberto D'Alesio, Francesco Murgia, and Cristian Pisano. Testing the universality of the Collins function in pion-jet production at RHIC. *Phys. Lett. B*, 773:300–306, 2017.

[212] Daniele P. Anderle, Tom Kaufmann, Marco Stratmann, Felix Ringer, and Ivan Vitev. Using hadron-in-jet data in a global analysis of D^* fragmentation functions. *Phys. Rev. D*, 96(3):034028, 2017.

[213] Alessandro Bacchetta, Marco Radici, and Lorenzo Rossi. Analogies between hadron-in-jet and dihadron fragmentation. *Phys. Rev. D*, 108(1):014005, 2023.

[214] Zhong-Bo Kang, Hongxi Xing, Fanyi Zhao, and Yiyu Zhou. Polarized fragmenting jet functions in inclusive and exclusive jet production. *JHEP*, 03:142, 2024.

[215] Xiaohui Liu, Felix Ringer, Werner Vogelsang, and Feng Yuan. Lepton-jet Correlations in Deep Inelastic Scattering at the Electron-Ion Collider. *Phys. Rev. Lett.*, 122(19):192003, 2019.

[216] Miguel Arratia, Youqi Song, Felix Ringer, and Barbara V. Jacak. Jets as precision probes in electron-nucleus collisions at the future Electron-Ion Collider. *Phys. Rev. C*, 101(6):065204, 2020.

[217] Miguel Arratia, Zhong-Bo Kang, Alexei Prokudin, and Felix Ringer. Jet-based measurements of Sivers and Collins asymmetries at the future electron-ion collider. *Phys. Rev. D*, 102(7):074015, 2020.

[218] Xiaohui Liu, Felix Ringer, Werner Vogelsang, and Feng Yuan. Lepton-jet Correlation in Deep Inelastic Scattering. *Phys. Rev. D*, 102(9):094022, 2020.

[219] Mohamed Abdallah et al. Azimuthal transverse single-spin asymmetries of inclusive jets and identified hadrons within jets from polarized pp collisions at $\sqrt{s}$ = 200 GeV. *Phys. Rev. D*, 106(7):072010, 2022.

[220] R. D. Field and R. P. Feynman. A Parametrization of the Properties of Quark Jets. *Nucl. Phys. B*, 136:1, 1978.

[221] Wouter J. Waalewijn. Calculating the Charge of a Jet. *Phys. Rev. D*, 86:094030, 2012.

[222] David Krohn, Matthew D. Schwartz, Tongyan Lin, and Wouter J. Waalewijn. Jet Charge at the LHC. *Phys. Rev. Lett.*, 110(21):212001, 2013.

[223] Zhong-Bo Kang, Xiaohui Liu, Sonny Mantry, and Ding Yu Shao. Jet Charge: A Flavor Prism for Spin Asymmetries at the EIC. *Phys. Rev. Lett.*, 125:242003, 2020.

[224] Hai Tao Li and Ivan Vitev. Jet charge modification in dense QCD matter. *Phys. Rev. D*, 101:076020, 2020.

[225] Zhong-Bo Kang, Andrew J. Larkoski, and Jinghong Yang. Towards a Nonperturbative Formulation of the Jet Charge. *Phys. Rev. Lett.*, 130(15):151901, 2023.

[226] Elke-Caroline Aschenauer, Kyle Lee, B. S. Page, and Felix Ringer. Jet angularities in photoproduction at the Electron-Ion Collider. *Phys. Rev. D*, 101(5):054028, 2020.

[227] Shen Fang, Shuo Lin, Ding Yu Shao, and Jian Zhou. Nucleon Tomography with Zero Jettiness. *Phys. Rev. Lett.*, 136(2):021901, 2026.

[228] Dingyu Shao. New Perspectives on Precision Nucleon Tomography. Talk at the 8th National Workshop on Heavy Flavor Physics and Quantum Chromodynamics, April 2026. Presentation slides, April 25, 2026, Chongqing University.

[229] Lucia Hackermueller, Klaus Hornberger, Bjoern Brezger, Anton Zeilinger, and Markus Arndt. Decoherence of matter waves by thermal emission of radiation. *Nature*, 427:711–714, 2004.

[230] Hai Tao Li and Ivan Vitev. Nuclear Matter Effects on Jet Production at Electron-Ion Colliders. *Phys. Rev. Lett.*, 126(25):252001, 2021.

[231] Hai Tao Li, Ze Long Liu, and Ivan Vitev. Heavy flavor jet production and substructure in electron-nucleus collisions. *Phys. Lett. B*, 827:137007, 2022.

[232] Kyle Lee, James Mulligan, Mateusz Płoskoń, Felix Ringer, and Feng Yuan. Machine learning-based jet and event classification at the Electron-Ion Collider with applications to hadron structure and spin physics. *JHEP*, 03:085, 2023.

[233] Hai Tao Li and Ivan Vitev. Inclusive heavy flavor jet production with semi-inclusive jet functions: from proton to heavy-ion collisions. *JHEP*, 07:148, 2019.

[234] Hai Tao Li and Ivan Vitev. Inverting the mass hierarchy of jet quenching effects with prompt b-jet substructure. *Phys. Lett. B*, 793:259–264, 2019.

[235] Shreyasi Acharya et al. Measurements of Groomed-Jet Substructure of Charm Jets Tagged by D0 Mesons in Proton-Proton Collisions at s=13 TeV. *Phys. Rev. Lett.*, 131(19):192301, 2023.

[236] Simone Caletti, Andrea Ghira, and Simone Marzani. On heavy-flavour jets with Soft Drop. *Eur. Phys. J. C*, 84(2):212, 2024.

[237] Prasanna K. Dhani, Oleh Fedkevych, Andrea Ghira, Simone Marzani, and Gregory Soyez. Heavy flavour jet substructure. *JHEP*, 02:046, 2025.

[238] Albert M Sirunyan et al. Measurement of the Splitting Function in pp and Pb-Pb Collisions at $\sqrt{s_{\rm NN}}$ = 5.02 TeV. *Phys. Rev. Lett.*, 120(14):142302, 2018.

[239] Albert M Sirunyan et al. Jet properties in PbPb and pp collisions at $\sqrt{s_{\rm NN}} = 5.02$ TeV. *JHEP*, 05:006, 2018.

[240] Morad Aaboud et al. Comparison of Fragmentation Functions for Jets Dominated by Light Quarks and Gluons from pp and Pb+Pb Collisions in ATLAS. *Phys. Rev. Lett.*, 123(4):042001, 2019.

[241] Shreyasi Acharya et al. Measurement of the groomed jet radius and momentum splitting fraction in pp and Pb−Pb collisions at $\sqrt{s_{NN}} = 5.02$ TeV. *Phys. Rev. Lett.*, 128(10):102001, 2022.

[242] M. S. Abdallah et al. Differential measurements of jet substructure and partonic energy loss in Au+Au collisions at $\sqrt{S_{NN}}$ =200 GeV. *Phys. Rev. C*, 105(4):044906, 2022.

[243] Shreyasi Acharya et al. Medium-induced modification of groomed and ungroomed jet mass and angularities in Pb–Pb collisions at sNN=5.02 TeV. *Phys. Lett. B*, 864:139409, 2025.

[244] Ivan Vitev, Simon Wicks, and Ben-Wei Zhang. A Theory of jet shapes and cross sections: From hadrons to nuclei. *JHEP*, 11:093, 2008.

[245] Yang-Ting Chien and Ivan Vitev. Towards the understanding of jet shapes and cross sections in heavy ion collisions using soft-collinear effective theory. *JHEP*, 05:023, 2016.

[246] Yacine Mehtar-Tani and Konrad Tywoniuk. Groomed jets in heavy-ion collisions: sensitivity to medium-induced bremsstrahlung. *JHEP*, 04:125, 2017.

[247] Yang-Ting Chien and Ivan Vitev. Probing the Hardest Branching within Jets in Heavy-Ion Collisions. *Phys. Rev. Lett.*, 119(11):112301, 2017.
[248] P. Caucal, E. Iancu, A. H. Mueller, and G. Soyez. Vacuum-like jet fragmentation in a dense QCD medium. *Phys. Rev. Lett.*, 120:232001, 2018.
[249] Guilherme Milhano, Urs Achim Wiedemann, and Korinna Christine Zapp. Sensitivity of jet substructure to jet-induced medium response. *Phys. Lett. B*, 779:409–413, 2018.
[250] P. Caucal, E. Iancu, and G. Soyez. Deciphering the z_g distribution in ultrarelativistic heavy ion collisions. *JHEP*, 10:273, 2019.
[251] J. Casalderrey-Solana, G. Milhano, D. Pablos, and K. Rajagopal. Modification of Jet Substructure in Heavy Ion Collisions as a Probe of the Resolution Length of Quark-Gluon Plasma. *JHEP*, 01:044, 2020.
[252] James Mulligan and Mateusz Ploskon. Identifying groomed jet splittings in heavy-ion collisions. *Phys. Rev. C*, 102(4):044913, 2020.
[253] Paul Caucal, Alba Soto-Ontoso, and Adam Takacs. Dynamically groomed jet radius in heavy-ion collisions. *Phys. Rev. D*, 105(11):114046, 2022.